

The Galactic R Coronae Borealis stars: the C₂ Swan bands, the carbon problem, and the ¹²C/¹³C ratio

B. P. Hema¹, Gajendra Pandey¹, and David L. Lambert²

¹ Indian Institute of Astrophysics, Bangalore Karnataka 560034, India; hema@iiap.res.in,
pandey@iiap.res.in

² The W.J. McDonald Observatory, University of Texas at Austin, Austin, TX 78712-1083,
USA; dll@astro.as.utexas.edu

Received _____; accepted _____

ABSTRACT

Observed spectra of R Coronae Borealis (RCB) and hydrogen-deficient carbon (HdC) stars are analyzed by synthesizing the C₂ Swan bands (1,0), (0,0), and (0,1) using our detailed line list and the Uppsala model atmospheres. The (0,1) and (0,0) C₂ bands are used to derive the ¹²C abundance, and the (1,0) ¹²C/¹³C band to determine the ¹²C/¹³C ratios. The carbon abundance derived from the C₂ Swan bands is about the same for the adopted models constructed with different carbon abundances over the range: 8.5 (C/He = 0.1%), to 10.5 (C/He = 10%). Carbon abundances derived from C I lines are about a factor of 4 lower than the carbon abundance of the adopted model atmosphere over the same C/He interval, as reported by Asplund et al. (2000), who dubbed the mismatch between adopted and derived C abundance the ‘carbon problem’. In principle, the carbon abundances obtained from C₂ Swan bands and that assumed for the model atmosphere can be equated for a particular choice of C/He that varies from star to star. Then, the carbon problem for C₂ bands is eliminated. However, such C/He ratios are in general less than those of the EHe stars, the seemingly natural relatives to the RCB and HdC stars. A more likely solution to the C₂ carbon problem may lie in a modification of the model atmosphere’s temperature structure. The derived carbon abundances and the ¹²C/¹³C ratios are discussed in light of the double degenerate (DD) and the final flash (FF) scenarios.

Subject headings: Stars - abundances, Isotopic ratio- carbon, evolution of stars

1. Introduction

R Coronae Borealis (RCB) stars are a rare class of F- and G- type supergiants with remarkable photometric and spectroscopic peculiarities. The photometric peculiarity is that a RCB may fade rapidly in visual brightness by up to several magnitudes at unpredictable times and slowly return back to maximum light after an interval of weeks, months or even years. Most RCB stars stay for a longer time at maximum light than at minimum light. This fading is generally attributed to the formation of dust in the line of sight. Spectroscopic peculiarities are led by the very weak or undetectable hydrogen Balmer lines in their spectra. This indicates that they have a very H-poor atmosphere. This hydrogen deficiency but not the propensity to undergo optical declines is shared by other rare classes of stars: extreme helium (EHe) stars at the hotter end and hydrogen-deficient carbon (HdC) stars at the cooler end of the RCB temperature range.

Keys to understanding origins of RCB stars and their putative relatives have come from the determination and interpretation of the stars’ surface chemical compositions. Two proposed scenarios remain in contention. In one dubbed the double degenerate (DD) scenario, a helium white dwarf merges with a carbon-oxygen (C-O) white dwarf (Webbink 1984; Iben & Tutukov 1985). The close white dwarf binary results from mass exchange and mass loss of a binary system as it evolves from a pair of main sequence stars. The final step to the merger is driven by loss of angular momentum by gravitational waves (Renzini 1979). The envelope of the merged star is inflated to supergiant dimensions for a brief period. An alternative scenario dubbed the final flash (FF) scenario involves a single post-AGB star experiencing a final helium shell flash which causes the H-rich envelope to be ingested by the He shell. The result is the star becomes a hydrogen-deficient supergiant for a brief period, and is sometimes referred in this condition as a born-again AGB star (Renzini 1990).

For the RCB stars, determination of chemical compositions by Lambert & Rao (1994) and Asplund et al. (2000) suggested that the DD rather than the FF scenario gave the superior accounting of the determined elemental abundances. This conclusion has since been supported by the determination from analysis of CO infrared bands of a high ^{18}O (relative to ^{16}O) in cool RCBs and HdC stars (Clayton et al. 2005, 2007; García-Hernández et al. 2009, 2010). Additional evidence comes from high fluorine abundances in EHe (Pandey 2006) and RCB stars (Pandey et al. 2008).

In the case of the RCB stars, there is an unease about the results for the elemental abundance on account of ‘the carbon problem’ identified and discussed by Asplund et al. (2000). Since the continuous opacity in the optical is predicted to arise from the photoionization of neutral carbon from highly excited states, the strength of an optical C I line, also from a highly excited state, is predicted to be quasi-independent of atmospheric parameters such as effective temperature, surface gravity and metal abundance. Indeed, a C I line has a nearly constant strength across the RCB sample even as (for example) a Fe I or Fe II line may vary widely in strength from one star to the next. However, the predicted strength of a C I line is much stronger than its observed strength: if one were to choose to resolve this discrepancy by adjusting the line’s gf -value, it must be reduced by a factor of four or 0.6 dex on average. This discrepancy between predicted and observed C I line strengths is termed ‘the carbon problem’. Adjustment of the gf -values of the C I lines is not the only potential or even the preferred way to address the carbon problem.

In this paper, we present and discuss spectra showing the C₂ Swan bands in a sample of RCB and HdC stars. Our first goal is to compare predicted and observed strengths of C₂ Swan bands in RCB stars to see if they exhibit a carbon problem and if that problem differs from that shown by the C I lines. Our second goal is to look for $^{12}\text{C}^{13}\text{C}$ lines and determine the $^{12}\text{C}/^{13}\text{C}$ ratio. A high value of $^{12}\text{C}/^{13}\text{C}$ ratio is expected for the DD scenario,

but a low ratio seems likely for the FF scenario. High ratios or high lower limits on the isotopic ratio have been set for HdC stars: HD 137613 (Fujita & Tsuji 1977), HD 182040 (Climenthaga 1960; Fujita & Tsuji 1977). A limit of greater than 40 was set for RCrB (Cottrell & Lambert 1982). But the RCB star VCrA is apparently an exception with a reported low value of $^{12}\text{C}/^{13}\text{C}$ ratio: Rao & Lambert (2008) estimated the ratio at 4-10 for VCrA.

As expected, a low value of $^{12}\text{C}/^{13}\text{C}$ ratio is shown by the final flash object V4334Sgr (Sakurai’s object), the ratio is 2 to 5 (Asplund et al. 1997b; Pavlenko et al. 2004). However, the other objects which are thought to be final flash objects, like, FG Sge (Gonzalez et al. 1998) and V605 Aql (Lundmark 1921; Clayton & De Marco 1997), do not show the presence of $^{12}\text{C}^{13}\text{C}$ bands in their spectrum.

2. Observations

High resolution optical spectra of RCB/HdC stars at maximum light were obtained from the W. J. McDonald Observatory and the Vainu Bappu Observatory. The dates of observations, the visual validated magnitudes (AAVSO¹) and the signal-to-noise ratio per pixel of the spectra in the continuum near the 4737 \AA $^{12}\text{C}_2$ bandhead are given in Table 1. In addition to the RCB stars, a spectrum of γ Cyg was obtained at the McDonald Observatory. This F5Ib star is of similar spectral type to the warm RCBs such as RCrB.

The spectra from the McDonald Observatory were obtained with the 2.7-m Harlan J. Smith Telescope and Tull coudé cross-dispersed echelle spectrograph (Tull et al. 1995) at a resolving power of $\lambda/d\lambda = 60,000$. The spectra from the Vainu Bappu Observatory were obtained with the 2.34-m Vainu Bappu Telescope (VBT) equipped with the fiber-fed

¹<http://www.aavso.org>

cross-dispersed echelle spectrometer (Rao et al. 2005) and a $4K \times 4K$ CCD are at a resolving power of about 30,000.

3. Spectrum synthesis

Our analysis of the high-resolution spectra proceeds by fitting synthetic spectra to the observed spectra in several bandpasses providing lines of the C_2 Swan system. For the synthesis of the C_2 Swan bands, we use model atmospheres and as complete a line list as possible. In the following subsections we introduce the line lists for the C_2 Swan bands and the atomic lines blended with the C_2 bands and, finally, the procedure for computing the synthetic spectra.

3.1. The Swan bands

The C_2 Swan bands are detectable in all but the hottest RCB stars. They are not seen in either V3795 Sgr or XX Cam with effective temperatures of 8000 K and 7250 K, respectively. In our sample, they are first detectable in VZ Sgr at $T_{\text{eff}} = 7000$ K. The bands are very strong in the coolest RCB stars like U Aqr and the HdC stars. The leading bands of the three sequences: $\Delta\nu = +1, 0$, and -1 are each considered. All bands have blue-degraded bandheads. The (0,0) band of the $^{12}C_2$ molecule with its head at 5165 Å is the strongest band of the entire Swan system. The (1,0) and (0,1) bandheads are at 4737 Å and 5636 Å, respectively. All three bands are synthesized using detailed line lists including the blending atomic lines and appropriate model atmospheres. The (1,0), (0,0), and (0,1) $^{12}C_2$ bands are used to determine the C abundance and, hence, to assess the carbon problem. The (0,1) band is generally a superior indicator of the C abundance because it is less affected by blending atomic lines. However, the (1,0) band is the focus of efforts to determine the

$^{12}\text{C}/^{13}\text{C}$ ratio because the $^{12}\text{C}^{13}\text{C}$ bandhead is shifted to 4745 Å and, thus, 8 Å clear of the blue-degraded $^{12}\text{C}_2$ band. For the (0,0) and (0,1) bands, the $^{12}\text{C}^{13}\text{C}$ lines are mixed among the stronger $^{12}\text{C}_2$ lines.

Data required for synthesis of Swan bands include: wavelengths of the transitions, excitation energies of the lower levels, gf -values of the lines and the C_2 molecule’s dissociation energy. Accurate wavelengths for $^{12}\text{C}_2$ lines are taken from Phillips & Davis (1968). Excitation energies are computed from the molecular constants given by the latter reference. The wavelength shift between a $^{12}\text{C}^{13}\text{C}$ line and the corresponding $^{12}\text{C}_2$ line is calculated using standard formulae for the vibrational and rotational shifts (Herzberg & Phillips 1948; Stawikowski & Greenstein 1964; Russo et al. 2011). Predictions for the bandhead wavelength shifts were checked against the measurements by Pesic et al. (1983).

gf -values are calculated from the theoretical band oscillator strengths computed by Schmidt & Bacskaý (2007): $f(1,0) = 0.009414$, $f(0,0) = 0.03069$, and $f(0,1) = 0.01015$. These theoretical computations predict radiative lifetimes for the upper state of the Swan system that are within a few per cent of the accurate measurements by laser-induced fluorescence reported by Naulin et al. (1988). The C_2 dissociation energy is taken from an experiment involving multi-photon dissociation of acetylene: $D_0(\text{C}_2) = 6.297$ eV (Urdahl et al. 1991). Our molecular data for individual $^{12}\text{C}_2$ lines – gf -values and excitation energies – are in excellent agreement with values listed by Asplund et al. (2005) for their determination of the solar C abundance. For detailed molecular line lists used in our analyses of C_2 bands, including the wavelengths, J -values of the lower level, the lower excitation potentials, and the log gf -values, see Tables 2, 3, 4, 5, 6 and 7.

3.2. Atomic lines

In order to ensure a satisfactory synthesis of a RCB spectrum, an accounting for the atomic lines at the wavelengths covered by the C₂ bands is necessary, most especially for the (1,0) ¹²C¹³C bandhead which is always weak and generally seriously blended. The region 4729-4748 Å was given especial attention. The procedure applied to the (1,0) band was followed for the (0,0) and (0,1) bands.

Prospective atomic lines were first compiled from the usual primary sources: the Kurucz database ², the NIST database³, the VALD database⁴ and the comprehensive multiplet table for FeI (Nave et al. 1994). Our next step was to identify the atomic lines in the spectrum of γ Cyg, Arcturus, and the Sun and to invert their equivalent widths to obtain the product of a line’s *gf*-value and the element’s abundance. For lines of a given species (e.g., FeI), the assumption is that the relative *gf*-values obtained from these sources may be applied to a RCB spectrum synthesis but an adjustment may be needed to allow for an abundance difference between the source and the RCB. After the adjustment for abundance differences between the sources, the *gf*-values are in agreement within 0.1 dex (see Table 8 for the individual estimates of the *gf*-values as well as the adopted value). For most lines the *gf*-values adopted are those derived from γ Cyg spectrum. For the lines which are not resolved in γ Cyg spectrum, the *gf*-values are adopted from the solar spectrum.

Lines of C I present in all RCB spectra are not present in the reference spectra of γ Cyg, Arcturus and the Sun. The C I lines were identified using Moore (1993)’s multiplet

²<http://kurucz.harvard.edu>

³<http://www.nist.gov>

⁴<http://vald.astro.univie.ac.at>

table with gf -values taken from the NIST database. A C I line is betrayed by the fact that a given C I line has a similar strength in all RCB spectra. In this regard the feature coincident with the $^{12}\text{C}^{13}\text{C}$ (1,0) bandhead is unlikely to be a very weak unidentified C I line because its strength varies from star to star. Note, for example, the absence or near absence of this line in the spectra of V3795 Sgr and V854 Cen. Furthermore, this line is stronger in the spectrum of γ Cyg, where the C I lines are very weak.

Initially, elemental abundances for RCB stars were adopted from Asplund et al. (2000) and Rao & Lambert (2003). Then, equivalent widths were measured off our spectra and the abundances redetermined for RCB stars were found to be in good agreement with Asplund et al. (2000). In particular, we derived the Fe abundance from lines in the 4745-4810 Å window where C_2 contamination is minimal. The Fe abundances derived from these Fe I lines are in good agreement with the Fe abundances derived by Asplund et al. (2000) (see Table 9). These Fe abundances were adopted for deriving the $^{12}\text{C}/^{13}\text{C}$ ratios in RCB stars. The uncertainties on the Fe abundance is used to derive the upper and lower limits to $^{12}\text{C}/^{13}\text{C}$ ratios in RCB stars (including U Aqr). The metal abundances for the synthetic spectra are adopted from Asplund et al. (2000) for most of the stars. However, for V2552 Oph we adopt the abundances from Rao & Lambert (2003). We also assume the solar relative abundances with the correction of about +0.3 dex for the α -elements at these metallicities, if these abundances are not measured in these stars. Fe abundances are derived also for HdC stars and the cool RCB U Aqr.

3.3. Spectrum synthesis of the C_2 bands

For the spectrum synthesis, we used the line-blanketed H-deficient model atmospheres by Asplund et al. (1997a) and the UPPSALA spectrum synthesis BSYNRUN program. For equivalent width analysis we used EQWRUN program. The appropriate model atmosphere

for a given RCB star was chosen using the stellar parameters from Asplund et al. (2000): effective temperature T_{eff} , surface gravity $\log g$, and microturbulence ξ_t .

The stellar parameters for the cool RCB star U Aqr and HdC stars are adopted from Asplund et al. (1997a) and García-Hernández et al. (2009, 2010) and used with the MARCS model atmospheres (Gustafsson et al. 2008) provided by Kjell Eriksson (private communication) used by García-Hernández et al. (2009, 2010). For the four HdC stars and the cool RCB star U Aqr, we have derived the microturbulence (ξ_t) from Fe I lines in the region of 4750-4960 Å since there are no significant molecular bands in this wavelength region (Warner 1967). The microturbulent velocity derived from Fe I lines for U Aqr is $\xi_t = 5.0 \pm 2 \text{ km s}^{-1}$ and the Fe abundance is $\log \epsilon(\text{Fe}) = 6.7 \pm 0.3$, but adoption of a lower effective temperature, $T_{\text{eff}} = 5400 \text{ K}$, suggested by García-Hernández et al. (2010) gives an Fe abundance of 6.5 ± 0.3 . For HdC stars, the derived microturbulent velocities and Fe abundances are: for HD 137613, $\xi_t = 6.5 \pm 2 \text{ km s}^{-1}$ and $\log \epsilon(\text{Fe}) = 6.8 \pm 0.3$, for HD 182040, $\xi_t = 6.5 \pm 2 \text{ km s}^{-1}$ and $\log \epsilon(\text{Fe}) = 6.6 \pm 0.3$, for HD 173409, $\xi_t = 6.0 \pm 2 \text{ km s}^{-1}$ and $\log \epsilon(\text{Fe}) = 6.6 \pm 0.3$, and for HD 175893, $\xi_t = 6.0 \pm 2 \text{ km s}^{-1}$ and $\log \epsilon(\text{Fe}) = 6.7 \pm 0.3$. The other stellar parameters like T_{eff} and $\log g$, and the elemental abundances are judged from Warner (1967), Asplund et al. (1997a), and García-Hernández et al. (2009).

Stars with effective temperature less than or about 7000 K were selected for the analysis of their C_2 bands. The C_2 molecular bands were synthesized with the line lists discussed above. The synthesized spectrum was convolved with a Gaussian profile with a width that represents the combined effect of stellar macroturbulence and the instrumental profile. The synthesized spectrum is then matched to the observed spectrum by adjustment of the appropriate abundances.

4. The carbon abundance

If there were no carbon problem for C_2 bands, the ^{12}C abundance derived by fitting each $^{12}C_2$ band would equal the input C abundance of the adopted model atmosphere to within the margin implied by the uncertainties arising from the errors assigned to the model atmosphere parameters. (The changes in spectrum syntheses arising from uncertainties in the basic data for the Swan bands and in the carbon isotopic ratio are negligible.)

In Table 10 the derived C abundances from C_2 bands for the RCB stars are summarized for the three bands and for models with $C/He = 0.3, 1.0$ and 3.0% . Table 11 similarly gives C abundances for the four HdC stars and the cool RCB star U Aqr. In both Table 10 and 11 we also give the C abundance from the C I lines but only for $C/He=1\%$ models. For a given model, the three bands give the same C abundance to within 0.2 dex, a quantity comparable to the fitting uncertainty. Along the sequence of models from $C/He = 0.3$ to 3.0% , the derived C abundance decreases by about 0.2 dex for the warmest stars to 0.1 dex for the coolest stars or equivalently the carbon problem increases from the warmest stars to the coolest stars. A carbon problem exists for all models with C/He in the range from 0.3 to 3.0% . Extrapolation of the C abundances in Table 10 to lower input C/He ratio suggests that elimination of the C problem requires models with values of C/He across the range 0.3% (VZ Sgr, R CrB) to 0.03% (V2552 Oph, SU Tau). Table 11 suggests that $C/He \simeq 0.3\%$ may account for the HdC stars and cool RCB U Aqr. Adoption of $T_{\text{eff}} = 6000K$ for U Aqr suggests C/He of 10% , and not in line with that of HdC stars. Hence, The $T_{\text{eff}} = 5400K$ is adopted for U Aqr over the $T_{\text{eff}} = 6000K$. Discussion of this C/He range is postponed to Section 5.

By way of illustrating the fits of the synthetic spectra to observed spectra for the warm RCB stars, we show synthetic and observed spectra for SU Tau in Figures 1, and 2 for the (0,0) and (0,1) C_2 bands, respectively. A corresponding figure for the (1,0) figure is

shown later. The (0,1), (0,0) and (1,0) bands each highlight a different issue. For the HdC stars and the cool RCB U Aqr, the C_2 bands are very strong and the issues are somewhat different and related to the saturation of the lines.

For the (0,1) band, a ^{12}C abundance is found to fit well the entire illustrated region except that right at the bandhead the observed spectrum is shallower than that predicted. This mismatch is not peculiar to SU Tau and is insensitive to the choice of the C/He ratio. This best fit for SU Tau demands a C abundance of 8.1 or, equivalently, presents a C problem of 0.9 dex; the synthesis with a C abundance of 9.0 (i.e., zero C problem) is obviously a very poor representation of the observed spectrum.

Synthetic spectra for the (0,0) bands give results essentially identical to those for the (0,1) bands. The C abundance from the best-fitting synthesis as judged by the fit to the C_2 lines away from the bandhead is within 0.2 dex of the values from the (0,1) bands. The mismatch between synthesis and observation at the bandhead is greater than for the (0,1) band and extends over a greater wavelength interval than for the (0,1) band.

A special difficulty occurs at the (1,0) $^{12}C_2$ bandhead because there are strong atomic lines at and shortward of the bandhead. A line right at the head is a Fe I line and those shortward of the head are C I lines. These and weaker atomic lines make it difficult to distinguish the C_2 contribution to the spectrum from that of the atomic lines when the C_2 contribution is weak.

As long as the continuous opacity is provided by photoionization of neutral carbon, the carbon problem (see Tables 10 and 11) raised by the C I lines cannot be erased by changes to the stellar parameters. The original carbon problem referred to the mismatch between the observed and predicted strengths of C I lines: the latter were stronger than the former by an amount equivalent to about a 0.6 dex reduction in a line's gf -value. The star-to-star variation in this reduction across the RCB sample was small: for example, the C I problem

for the ten stars in Table 10 spanned the small interval of -0.3 to -0.9 with a mean value of -0.7 ± 0.1 (Asplund et al. 2000). This carbon problem’s magnitude is almost independent of the assumed C/He ratio for which the model is constructed, i.e., the difference between the assumed and derived C abundance is maintained as C/He is adjusted. The C I lines included in present syntheses confirm the C problem. With gf -values from the NIST database, these lines demand a gf -value decrease of 0.5 to 0.8 dex for the eleven stars in Table 10 and the five stars in Table 11.

4.1. The $^{12}\text{C}/^{13}\text{C}$ ratio

The $^{12}\text{C}^{13}\text{C}$ molecule’s contribution to the spectra is assessed from the (1,0) band. Unfortunately, there is an unidentified atomic line coincident with the $^{12}\text{C}^{13}\text{C}$ bandhead. Syntheses show that this atomic line is a major contributor to the stellar feature in most stars. There is also strong atomic blending of the $^{12}\text{C}_2$ bandhead but the ^{12}C abundance is provided securely from the (0,0) and (0,1) bands. Given these complications, our focus is on determining whether the $^{12}\text{C}/^{13}\text{C}$ ratio is close to the CN-cycle equilibrium ratio ($= 3.4$), as might be anticipated for a star produced by the FF scenario, or is a much higher value, as might be provided from the DD scenario. The intensity of a line from the heteronuclear $^{12}\text{C}^{13}\text{C}$ molecule and the corresponding line from the homonuclear $^{12}\text{C}_2$ molecule are related as $I(12-13) = 2I(12-12)/R$ where R is the $^{12}\text{C}/^{13}\text{C}$ ratio.

Of particular concern to a determination of the $^{12}\text{C}/^{13}\text{C}$ ratio is the atomic line at 4744.39 \AA which is coincident with the (1,0) $^{12}\text{C}^{13}\text{C}$ bandhead. This line is present in the spectrum of γ Cyg, also of the Sun and Arcturus. A line at this wavelength is present in spectra of the hotter RCB stars (V3795 Sgr and XX Cam) whose spectra show no sign of the stronger (0,0) C_2 band at 5165 \AA . The interfering line is unidentified in Hinkle et al. (2000)’s

Arcturus atlas. The line list given at the ccp7 website⁵ identifies the line as arising from a lower level in Fe I at 4.50 eV but such a line and lower level is not listed by Nave et al. (1994) in their comprehensive study of the Fe I spectrum. The line list given in ccp7 is from Bell & Gustafsson (1989), an unpublished line list. Although this line is assigned in Table 8 to this (fictitious?) Fe I transition, the lack of a positive identification is not a serious issue except, as we note below, perhaps for the minority RCB stars. Given that the gf -value of the line is fixed from the line’s strength in spectra of stars that span the temperature range of the RCBs (γ Cyg, Arcturus, and the Sun), alternative identifications have little effect on the predicted strength of the line in a RCB or a HdC star. We assume it is a Fe I line and predict its strength from the inferred gf -value (Table 8) and the Fe abundance derived from a sample of Fe I line in the same region (see above). Table 9 lists our derived Fe abundance, the Fe abundance from Asplund et al. (2000), and the Fe abundance obtained on the assumption that the entire $^{12}\text{C}^{13}\text{C}$ bandhead is attributable to the Fe I line. There is good agreement between our Fe abundance and that derived from different spectra by Asplund et al. (2000). Perfect agreement would not be expected for several reasons: for example, the stars are somewhat variable even out of decline and our spectra are not those analysed by Asplund et al. (2000). The difference between the mean Fe abundance and the abundance required to fit the feature at the $^{12}\text{C}^{13}\text{C}$ bandhead is a rough measure of the inferred molecular contribution to the feature.

Stars are discussed in the order of decreasing effective temperature. For all the stars synthetic spectra are computed for a model with the parameters given in Table 12 and with $\text{C}/\text{He} = 1.0\%$. The $^{12}\text{C}_2$ bands are fitted and then several syntheses are computed for various values of the isotopic ratio R . The estimates of $^{12}\text{C}/^{13}\text{C}$ ratio are given in Table 12.

VZ Sgr: Observed and synthetic spectra around the (1,0) band are shown in Figure 3

⁵<http://ccp7.dur.ac.uk/ccp7/DATA/lines.bell.tar.Z>

for this minority RCB star. At 4745 Å, the atomic line (here assumed to be the Fe I line from Table 8) is too weak to account for the observed feature; Table 9 shows that the Fe abundance must be increased by about 1 dex to remove the necessity for a contribution from $^{12}\text{C}^{13}\text{C}$. A contribution from $^{12}\text{C}^{13}\text{C}$ seems necessary with $R \simeq 3-6$, a value suggestive of CN-cycling. The observed $^{12}\text{C}^{13}\text{C}$ band is very weak, and taking into account the signal-to-noise ratio, the expected band asymmetry is not evident. The blending Fe I line at the $^{12}\text{C}^{13}\text{C}$ bandhead further removes the expected asymmetry. However, the blending Fe I line is very weak, the residual spectrum, observed/synthesis (pure C_2 with $R = 4$), suggests the presence of the contaminating line at 4744.39 Å within the uncertainties.

Since the relative metal abundances for VZ Sgr, a minority RCB, are non-solar (Lambert & Rao 1994), the identity of the 4745 Å atomic line may affect the conclusion that this line is an unimportant contributor to the molecular bandhead. For example, VZ Sgr is a minority RCB especially rich in Si and S ($[\text{Si}/\text{Fe}] \sim [\text{S}/\text{Fe}] \sim 2$) and a blending line from these elements may reduce the need for a $^{12}\text{C}^{13}\text{C}$ contribution. However, a search of multiplet tables of Si I (Martin & Zalubas 1983) and S I (Martin et al. 1990; Kaufman & Martin 1993) did not uncover an unwanted blend. Thus, we suppose that VZ Sgr is rich in ^{13}C .

UX Ant: There is a strong (1,0) $^{12}\text{C}_2$ contribution to the spectrum. The predicted profile of the bandhead is broader than the observed head which is distorted by very strong cosmic ray hits on the raw frame. The Fe I line is predicted to be a weak contributor to the feature at the $^{12}\text{C}^{13}\text{C}$ wavelength. Values of R in the range 14 to 20 fit the observed feature quite clearly, a synthesis with $R = 3.4$ provides a bandhead that is incompatible with the observed head (Figure 4).

RS Tel: Observed and synthetic spectra shown in Figure 4 indicate that the Fe I line at the $^{12}\text{C}^{13}\text{C}$ band head accounts well for the observed feature and thus $R > 60$ is all that

can be said for the carbon isotopic ratio from this spectrum of relatively low S/N ratio.

R CrB: Figure 5 shows observed and synthetic spectra. The Fe I line at the $^{12}\text{C}^{13}\text{C}$ bandhead accounts for the observed feature. Given that the identity of the line’s carrier is uncertain, a conservative view must be that $^{12}\text{C}^{13}\text{C}$ contributes negligibly to the observed feature and $R > 40$ is estimated. It is clear, however, that $R = 3.4$ is excluded as a possible fit.

V2552 Oph: The spectrum of this recently discovered RCB is very similar to that of R CrB (Rao & Lambert 2003) but for its stronger Ni lines and weaker C_2 bands (Figure 1 of Rao & Lambert (2003)). The $^{12}\text{C}_2$ bandhead is very largely obscured by the overlying Fe I line. The apparent $^{12}\text{C}^{13}\text{C}$ bandhead is almost entirely reproduced by the atomic line. A high R value cannot be rejected but $R = 3.4$ may be excluded (Figure 5). $R > 8$ is our estimate.

V854 Cen: This RCB with low metal abundances provides a clean spectrum in the the region of the (1,0) Swan bands (Figure 6). The $^{12}\text{C}_2$ head is well fitted with a synthetic spectrum. Very high S/N ratio spectra are necessary to set strict limits on the $^{12}\text{C}^{13}\text{C}$ bandhead but it is clear that the blending Fe I line is a weak contributor; the Fe abundance must be increased by 1.5 dex to eliminate the need for a $^{12}\text{C}^{13}\text{C}$ contribution. A ratio $R = 3.4$ is firmly excluded. Values of R in the range 16 to 24 are suggested.

V482 Cyg: The Fe I line accounts well for the observed feature (Figure 6) with a lower limit for the isotopic ratio $R > 100$.

SU Tau: At the $^{12}\text{C}^{13}\text{C}$ bandhead, the atomic line makes a dominant contribution but the profile of the observed feature suggests that the Swan band is contributing to the blue of the atomic line (Figure 7): R seems to be > 24 . The $R = 3.4$ synthetic spectrum is clearly rejected as a fit to the observed spectrum.

V CrA: The FeI line at the $^{12}\text{C}^{13}\text{C}$ bandhead, and the expected band asymmetry, is seemingly quite unimportant but V CrA is another minority RCB so that the identity of the line’s carrier may be relevant here (see above notes on VZ Sgr). The $^{12}\text{C}_2$ band is quite strong (Figure 7). With the blending line assigned to FeI, the observed $^{12}\text{C}^{13}\text{C}$ bandhead is well fit with $R \simeq 8$ to 10. Our derived $^{12}\text{C}/^{13}\text{C}$ ratio is in agreement with the upper limit of the range set by Rao & Lambert (2008) from the same spectrum. Note that an additional line about 0.6 \AA to the blue of the $^{12}\text{C}^{13}\text{C}$ bandhead is seen in this spectrum.

GU Sgr: Presence of the $^{12}\text{C}^{13}\text{C}$ band is doubtful because atomic lines may account fully for the bandhead and the region just to the blue: R seems to be in the range >40 (Figure 8).

FH Sct: Spectrum synthesis shows that $^{12}\text{C}_2$ makes a minor contribution to the observed spectrum (Figure 8) but the ^{12}C abundance may be established from the (0,0) and (0,1) bands. The ratio $R > 14$ may be set and the CN-cycle’s limit of $R=3.4$ is excluded.

U Aqr: The (1,0) $^{12}\text{C}_2$ band is so strong (Figure 9) that the uncertainty over R is dominated by the derivation of the ^{12}C abundance from the very saturated (1,0) $^{12}\text{C}_2$ lines. The carbon abundance from (the also saturated) (0,1) C_2 band is used with the (1,0) $^{12}\text{C}^{13}\text{C}$ blend to derive the $^{12}\text{C}/^{13}\text{C}$ ratio. The Fe abundance is derived from several lines longward of the (1,0) $^{12}\text{C}^{13}\text{C}$ bandhead. A $^{12}\text{C}/^{13}\text{C}$ ratio in the range 110 to 120 is obtained.

HdC stars: Syntheses of the (1,0) band are shown in Figures 10- 11 for the four HdC stars with the ^{12}C abundance set in each case by the fit to the (0,1) band (see Figure 12 for a typical fit). In contrast to U Aqr, the $^{12}\text{C}^{13}\text{C}$ bandhead is well fit by the blending atomic lines with the Fe abundance obtained from lines longward of the bandhead. The derived $^{12}\text{C}/^{13}\text{C}$ ratio is >100 for HD 137613, >400 for HD 182040, >100 for HD 175893, and >60 for HD 173409.

5. Discussion - C₂ and the Carbon Problem

The carbon problem as it appears from the analysis of C I lines is discussed fully by Asplund et al. (2000). In brief, when analysed with state-of-the-art H-poor model atmospheres (Asplund et al. 1997a) constructed for a C/He ratio (= 1%) representative of EHe stars where direct determinations of C and He abundances are possible, the C I lines return a C abundance that is about 0.6 dex less than the input abundance of $\log \epsilon(\text{C}) = 9.5$. The derived abundance varies little from star-to-star: 13 of the 17 analysed RCBs have abundances between 8.8 and 9.0 and the mean from the set of 17 is 8.9 ± 0.2 . A similar result is apparent from Tables 10 and 11 where the C abundance from C I lines from our spectrum syntheses is quoted. The discrepancy of 0.6 dex between assumed and derived C abundance is the (C I) carbon problem. As the C/He ratio of a model atmosphere is adjusted, the carbon problem (i.e., the 0.6 dex difference between assumed and derived C abundances) persists until a low C/He reached. This persistence arises because the continuous opacity arises from photoionization of neutral carbon from excited levels.

Tables 10 and 11 also show that the C₂ bands exhibit a carbon problem but one that differs from that shown by the C I lines in several ways: (i) the C abundance from C₂ bands is almost independent of the assumed C/He ratio unlike the abundance from C I lines; (ii) the star-to-star spread in C abundances from C₂ bands is larger than found from the C I lines; (iii) the C abundance from C₂ bands is somewhat more sensitive than that from C I lines to changes in the adopted atmospheric parameters as reflected by Table 13 where models spanning the effective temperature and surface gravity uncertainties suggested by Asplund et al. (2000) are considered.

Taken in complete isolation, inspection of Table 10 suggests that a C/He ratio of less than 0.3% can be found for which the ratio adopted in the construction of the model atmosphere is equal to that derived from the C₂ bands. For the RCB stars, Table 10

suggests C/He ratios running from about 0.3% for VZ Sgr and R CrB down to 0.03% for GU Sgr and FH Sct. For the HdC stars (Table 11), a C/He of slightly larger than 0.1% is suggested. However, Asplund et al. (2000) remark that $C/He \leq 0.05\%$ is required to eliminate the C I carbon problem by lowering the carbon abundance to the point that photoionization of neutral carbon no longer is the dominant opacity source.

Resolution of the carbon problems by invoking low C/He ratios deserves to be tested fully by constructing model atmospheres with lower C/He ratios and appropriate abundances for other elements and determining the C abundances from C I and C₂ lines. Asplund et al. (2000) recognized this possible way to address the C I carbon problem but discounted it on several grounds: (i) removal of carbon photoionization as the dominant continuous opacity makes it difficult to account for the near-uniformity of the C I equivalent widths across the RCB sample, especially as O abundance varies from star-to-star; (ii) an inverse carbon problem is created for the C II lines at 6578 Å and 6582 Å which are seen in the hottest RCBs; and (iii) these low C/He ratios for RCB stars are at odds with the higher ratios obtained directly from He and C lines for EHe stars which one assumes are intimate relatives of the RCB and HdC stars. Asplund et al. (2000) noted that published analyses of EHe stars gave the mean $C/He = 0.8 \pm 0.3\%$ over a range 0.3-1.0% with three unusual EHe stars providing much lower ratios (0.002% to 0.2%). Pandey et al. (2006) confirmed the C/He ratios for the leading group of EHe stars. From the following references (Pandey et al. 2001, 2006; Pandey & Lambert 2011; Jeffery et al. 1998; Drilling et al. 1998; Pandey & Reddy 2006; Jeffery & Heber 1993; Jeffery et al. 1999; Harrison & Jeffery 1997), that also includes the recent analyses of these EHe stars, the mean value of $C/He = 0.6 \pm 0.3\%$ is noted.

The RCB-EHe mismatch of their C/He ratios invites two responses: (i) the carbon problems for the RCB stars should be resolved on the assumption that their C/He ratios

and those of the EHe stars span similar ranges; or, (ii) as a result of different evolutionary paths, the C/He ratios of RCB and EHe stars span different ranges.

After considering a suite of possible explanations for their carbon problem, Asplund et al. (2000) proposed that the actual atmospheres of the RCB stars differed from the theoretical atmospheres in that the temperature gradient was flatter than predicted. Hand-crafted atmospheres were shown to solve the C I carbon problem. However, the issue of accounting for the additional heating and cooling of the hand-crafted atmospheres was left unresolved. In principle, the change in the temperature structure – a heating at modest optical depths – will require a higher C abundance to account for the C₂ bands so that the C I and C₂ carbon problems might be both eliminated.

Further exploration of the carbon problem was pursued by Pandey et al. (2004) who observed the 8727 Å and 9850 Å [C I] lines in a sample of RCB stars. The 8727 Å line gives a more severe carbon problem than the C I lines, say 1.2 dex versus 0.6 dex for C/He=1.0% model atmospheres. In part, this difference might be reduced by a revision of the effective temperature scale because the [C I] line being of low excitation potential has a temperature dependence relative to the continuous carbon opacity from highly excited levels. The 9850 Å line may give a similar carbon problem to the C I lines or the forbidden line may be blended with an unidentified line. To account for the 8727 Å carbon problem, Pandey et al. (2004) considered introducing a chromospheric temperature rise to the theoretical model photospheres. Such a chromosphere with LTE produces emission at the C₂ bandheads and offers a qualitative explanation for the fact that the best-fitting synthetic spectra from the theoretical photospheres (i.e., no chromospheric temperature rise) are deeper than the observed spectra at the bandheads.

Analysis of the C₂ bands suggests a novel clue to the C₂ carbon problem. As Figure 13 shows the C abundance from the C₂ bands is correlated with the O abundance derived

by Asplund et al. (2000) from O I and/or [O I] lines. The points are distributed about the relation $C/O \sim 1$. (The C abundance from the C I lines is not well correlated with the O abundance and most points fall below the $C/O = 1$ locus). In Figure 14, the EHe stars are plotted along with RCB stars. The RCB stars may connect those EHe stars of very low C/He with the majority of higher C/He.

Perhaps a more powerful clue is the fact that the Fe abundance of the RCB and HdC stars is uniformly sub-solar. The mean Fe abundance excluding the minority RCBs is 6.5 or 1.0 dex less than the solar Fe abundance. EHe stars show a similar spread and mean Fe abundance of 6.7 (Jeffery et al. 2011).

6. Discussion - The $^{12}\text{C}/^{13}\text{C}$ ratio and the origin of the RCBs

Discussion of the determinations of the $^{12}\text{C}/^{13}\text{C}$ ratio may be focussed on three main points.

First, the ratio is low in the two minority RCBs VZ Sgr and V CrA. Unless there is an unidentified line from an element with an overabundance in a minority RCB star, VZ Sgr has a $^{12}\text{C}/^{13}\text{C}$ ratio equal within the measurement uncertainty to the equilibrium ratio for the H-burning CN-cycle. The ratio is higher ($\simeq 8$) for V CrA but considerably lower than the upper limits set for majority RCBs. (Rao & Lambert (2008) gave the ratio as 3.4 for V CrA but apparently did not include the factor of two arising from the fact that $^{12}\text{C}^{13}\text{C}$ is not a homonuclear molecule, i.e., 3.4 should be 6.8.) In some respects, V854 Cen is a minority RCB star and its $^{12}\text{C}/^{13}\text{C}$ ratio of 18 is also generally lower than representative upper limits for majority RCB stars.

Second, the $^{12}\text{C}/^{13}\text{C}$ ratio for all majority RCBs is much larger than the equilibrium

ratio for the CN-cycle.⁶

Third, there appears to be a range in the $^{12}\text{C}/^{13}\text{C}$ ratios among majority RCBs. The star with the lowest ratio appears to be UX Ant (Figure 4) for which the predicted blend of atomic lines at the (1,0) $^{12}\text{C}^{13}\text{C}$ bandhead accounts for less than half of the strength of the observed absorption feature. Similarly for U Aqr, the atomic lines at the bandhead account for about half of the observed feature but because the C_2 lines are strong the isotopic bandhead translates to the ratio $^{12}\text{C}/^{13}\text{C} \simeq 110$. For these cases at least, it seems likely that the $^{12}\text{C}^{13}\text{C}$ bandhead is present in our spectra. Within the uncertainties associated with the blend of atomic lines, other RCBs yield a lower limit to the isotopic ratio. This limit is highest for the HdCs where the C_2 bands are very strong. Note how the atomic lines account remarkably well for the observed spectrum between the $^{12}\text{C}_2$ and $^{12}\text{C}^{13}\text{C}$ (1,0) bandheads.

Our results are in good agreement with published results for the few stars previously analysed (Table 12). In the case of R CrB, Cottrell & Lambert (1982) determined a lower limit of 40 from the C_2 (0,1) band. Fujita & Tsuji (1977) from spectra of the CN Red system set lower limits of 500 for HD 137613 and >100 for HD 182040. The latter limit was also reported by Climenhaga (1960) from high-resolution photographic spectra of C_2 bands. Lower limits set by García-Hernández et al. (2009, 2010) are not competitive with those from CN or our limits from C_2 .

Prospects for a low $^{12}\text{C}/^{13}\text{C}$ ratio in the atmosphere of a product of the DD scenario are dim. In the scenario’s cold version (i.e., no nucleosynthesis as a result of the merger), the C is provided by the He shell of the C-O white dwarf and quite likely also by layers

⁶We note that Goswami et al. (2010)’s observation that the ratio is about 3.4 for U Aqr is incompatible with our spectra by simple inspection of Figure 9.

of the C-O core immediately below the He shell. The latter contribution will be devoid of ^{13}C . In the He shell, ^{13}C may be present in the outermost layers as a result of penetration of protons from the H-rich envelope of the former AGB star into the He shell. Very slow penetration results in the build up of a $^{12}\text{C}/^{13}\text{C}$ ratio of about three and inhibits somewhat the conversion of the ^{13}C to ^{14}N , as usually occurs in the CN-cycle. This mechanism sustains the favored neutron source for the *s*-process in AGB stars; the $^{13}\text{C}(\alpha, n)^{16}\text{O}$ is the neutron source. The He is provided almost entirely by the He white dwarf which will have very little carbon but abundant nitrogen as a result of H-burning by the CNO-cycles.

A cold merger of the He white dwarf with the He shell of the C-O white dwarf results in a C/He ratio (see Pandey & Lambert (2011), eqn. 1)

$$\frac{\text{C}}{\text{He}} \simeq \frac{A(\text{He})}{A(\text{C})} \frac{\mu(\text{C})_{\text{C-O:He}} M(\text{C-O:He})}{M(\text{He})} \quad (1)$$

where $\mu(\text{C})_{\text{C-O:He}}$ is the mass fraction of ^{12}C in the He shell, $M(\text{C-O:He})$ is the mass of the He shell and $M(\text{He})$ is the mass of the He white dwarf. With plausible values for the quantities on the right-hand side of the equation, i.e., $\mu(\text{C})_{\text{C-O:He}} \simeq 0.2$, $M(\text{C-O:He}) \simeq 0.02M_{\odot}$, and $M(\text{He}) \simeq 0.3M_{\odot}$, one obtains $\text{C/He} \simeq 0.4\%$, a value at the lower end of the C/He range found for EHe stars. Additional ^{12}C is likely provided by mixing with the layers of the C-O white dwarf immediately below the He shell.

The attendant $^{12}\text{C}/^{13}\text{C}$ ratio will be a maximum if these latter contributions are absent. Then, this ratio will depend on the fraction of the He shell over which ^{13}C is abundant (relative to ^{12}C), say $^{12}\text{C}/^{13}\text{C} \sim 3/f_{13}$ where f_{13} is the fraction of the He shell which is rich in ^{13}C . For $f_{13} \sim 0.1$ and 0.01 , the predicted isotopic ratio is 30 and 300, respectively. These estimates must be increased when the mixing at the merger includes the layers of the C-O white dwarf immediately below the He shell.

At present, there are no reliable *ab initio* calculations of the mass of the ^{13}C -rich layer in the He shell of an AGB star. Additionally, one is making a bold assumption that the He shell of the C-O white dwarf which accepts merger with the He white dwarf resembles the He shell of a AGB star. Mass estimates relevant to an AGB star may be obtained by the fit to observed *s*-process abundances. Gallino et al. (1998) suppose that the ^{13}C rich layer amounts to about 1/20 of the mass in a typical thermal pulse occurring in the He shell. With $f_{13} \simeq 0.05$, the isotopic ratio is 60. Interestingly, this is consistent with our inferred range. This will increase as the C-O white dwarf contributes to the mixing. Destruction of ^{13}C by α particles may occur in a ‘hot’ phase during the merger and thus also raise the isotopic ratio; the $^{13}\text{C}(\alpha, n)$ destruction rate is roughly a factor of 100 faster than the $^{14}\text{N}(\alpha, \gamma)$ rate providing ^{18}O . The low isotopic ratio for minority RCB stars – VZ Sgr, and V CrA – are unexplained as are their distinctive elemental abundances.

7. Concluding remarks

The C_2 Swan bands are present in spectra of the HdC stars and in all but the hottest RCB stars. Analysis of these bands provides an alternative to the C I lines of providing estimates of the C abundance and in addition provide an opportunity to estimate the $^{12}\text{C}/^{13}\text{C}$ ratio. When analysed with Uppsala model atmospheres, the C_2 bands return a C abundance that is almost independent of the C/He ratio assumed in construction of the model atmosphere. If consistency between assumed and derived C abundances is demanded, the C_2 bands imply C/He ratios across the RCB and HdC sample run in the range 0.03% to 0.3%, a range that is notably lower than the range 0.3–1.0% found from a majority of EHes. This mismatch, if not a reflection of different modes of formation, implies that the C abundances for RCB and HdC stars are subject to a systematic error. Therefore, it appears that a version of the carbon problem affecting the C I lines (Asplund et al. 2000) applies to

the C_2 lines. Although alternative explanations can not yet be totally eliminated, it appears that higher order methods of model atmosphere construction are needed in order to check that Asplund et al.’s suggestion of the real atmospheres have a flatter temperature gradient than predicted by present state-of-the-art model atmospheres. Nonetheless, that the carbon abundances derived from C_2 Swan bands are the real measure of the carbon abundances in these stars cannot be ruled out.

There is evidence for the presence of detectable amounts of ^{13}C in the spectra of a few RCB stars and especially for the minority RCB stars. For the other RCBs and the HdC stars, lower limits are set on the carbon isotopic ratio. Apart from the minority RCB stars, the estimates of the carbon isotopic ratio are consistent with simple predictions for a cold merger of a He white dwarf with a C-O white dwarf.

The minority RCB stars are an enigma. Their distinctive pattern of elemental abundances remains unaccounted for; for example, V CrA has a Fe deficiency of 2 dex but $[Si/Fe] \sim [S/Fe] \sim [Sc/Fe] \simeq 2$ with $[Na/Fe] \sim [Mg/Fe] \sim 1$ (Rao & Lambert 2008). Add to these anomalies, the $^{12}C/^{13}C$ ratio is much lower than found for the majority RCB stars unless the (1,0) Swan $^{12}C^{13}C$ bandhead is blended with an as yet unidentified atomic line whose strength is unsuspected from examination of the spectra of majority RCB stars. The enigma calls for additional observational insights.

We thank Kjell Eriksson and Anibal García-Hernández for the H-deficient models of the cool stars, particularly Kjell Eriksson for providing these models in our required format. We thank Kameswara Rao for providing us the spectra of V854 Cen and V CrA. We also thank Nils Ryde for making available the C_2 line list by Querci et al. (1971) as a sample. DLL wishes to thank the Robert A. Welch Foundation of Houston, Texas for support through grant F-634.

REFERENCES

- Asplund, M., Grevesse, N., Sauval, A. J., Allende Prieto, C., & Blomme, R. 2005, *A&A*, 431, 693
- Asplund, M., Grevesse, N., Sauval, A. J., & Scott, P. 2009, *ARA&A*, 47, 481
- Asplund, M., Gustafsson, B., Kiselman, D., & Eriksson, K. 1997a, *A&A*, 318, 521
- Asplund, M., Gustafsson, B., Lambert, D. L., & Kameswara Rao, N. 1997b, *A&A*, 321, L17
- Asplund, M., Gustafsson, B., Lambert, D. L., & Rao, N. K. 2000, *A&A*, 353, 287
- Bell, R. A., & Gustafsson, B. 1989, *MNRAS*, 236, 653
- Clayton, G. C., & De Marco, O. 1997, *AJ*, 114, 2679
- Clayton, G. C., Geballe, T. R., Herwig, F., Fryer, C., & Asplund, M. 2007, *ApJ*, 662, 1220
- Clayton, G. C., Herwig, F., Geballe, T. R., Asplund, M., Tenenbaum, E. D., Engelbracht, C. W., & Gordon, K. D. 2005, *ApJ*, 623, L141
- Climenhaga, J. L. 1960, *AJ*, 65, 50
- Cottrell, P. L., & Lambert, D. L. 1982, *ApJ*, 261, 595
- Drilling, J. S., Jeffery, C. S., & Heber, U. 1998, *A&A*, 329, 1019
- Fujita, Y., & Tsuji, T. 1977, *PASJ*, 29, 711
- Gallino, R., Arlandini, C., Busso, M., Lugaro, M., Travaglio, C., Straniero, O., Chieffi, A., & Limongi, M. 1998, *ApJ*, 497, 388
- García-Hernández, D. A., Hinkle, K. H., Lambert, D. L., & Eriksson, K. 2009, *ApJ*, 696, 1733

- García-Hernández, D. A., Lambert, D. L., Kameswara Rao, N., Hinkle, K. H., & Eriksson, K. 2010, *ApJ*, 714, 144
- Gonzalez, G., Lambert, D. L., Wallerstein, G., Rao, N. K., Smith, V. V., & McCarthy, J. K. 1998, *ApJS*, 114, 133
- Goswami, A., Karinkuzhi, D., & Shantikumar, N. S. 2010, *ApJ*, 723, L238
- Gustafsson, B., Edvardsson, B., Eriksson, K., Jørgensen, U. G., Nordlund, Å., & Plez, B. 2008, *A&A*, 486, 951
- Harrison, P. M., & Jeffery, C. S. 1997, *A&A*, 323, 177
- Herzberg, G., & Phillips, J. G. 1948, *ApJ*, 108, 163
- Hinkle, K., Wallace, L., Valenti, J., & Harmer, D. 2000, *Visible and Near Infrared Atlas of the Arcturus Spectrum 3727-9300 Å*, ed. Hinkle, K., Wallace, L., Valenti, J., & Harmer, D.
- Iben, Jr., I., & Tutukov, A. V. 1985, *ApJS*, 58, 661
- Jeffery, C. S., Hamill, P. J., Harrison, P. M., & Jeffers, S. V. 1998, *A&A*, 340, 476
- Jeffery, C. S., & Heber, U. 1993, *A&A*, 270, 167
- Jeffery, C. S., Hill, P. W., & Heber, U. 1999, *A&A*, 346, 491
- Jeffery, C. S., Karakas, A. I., & Saio, H. 2011, *MNRAS*, 414, 3599
- Kaufman, U., & Martin, W. C. 1993, *Journal of Physics Conference Series*, 22, 279
- Kipper, T. 2002, *Baltic Astronomy*, 11, 249
- Lambert, D. L., & Rao, N. K. 1994, *Journal of Astrophysics and Astronomy*, 15, 47

- Luck, R. E., & Lambert, D. L. 1981, *ApJ*, 245, 1018
- Lundmark, K. 1921, *PASP*, 33, 314
- Martin, W. C., & Zalubas, R. 1983, *Journal of Physical and Chemical Reference Data*, 12, 323
- Martin, W. C., Zalubas, R., & Musgrove, A. 1990, *Journal of Physical and Chemical Reference Data*, 19, 821
- Moore Ch. E., 1993, in Gallagher J. W., ed., *CRC Series in Evaluated Data in Atomic Physics, Tables of Spectra of Hydrogen, Carbon, Nitrogen, and Oxygen Atoms and Ions*. CRC Press, Boca Raton
- Naulin, C., Costes, M., & Dorthe, G. 1988, *Chemical Physics Letters*, 143, 496
- Nave, G., Johansson, S., Learner, R. C. M., Thorne, A. P., & Brault, J. W. 1994, *ApJS*, 94, 221
- Pandey, G. 2006, *ApJ*, 648, L143
- Pandey, G., Kameswara Rao, N., Lambert, D. L., Jeffery, C. S., & Asplund, M. 2001, *MNRAS*, 324, 937
- Pandey, G., & Lambert, D. L. 2011, *ApJ*, 727, 122
- Pandey, G., Lambert, D. L., Jeffery, C. S., & Rao, N. K. 2006, *ApJ*, 638, 454
- Pandey, G., Lambert, D. L., & Rao, N. K. 2008, *ApJ*, 674, 1068
- Pandey, G., Lambert, D. L., Rao, N. K., Gustafsson, B., Ryde, N., & Yong, D. 2004, *MNRAS*, 353, 143
- Pandey, G., & Reddy, B. E. 2006, *MNRAS*, 369, 1677

- Pavlenko, Y. V., Geballe, T. R., Evans, A., Smalley, B., Eyres, S. P. S., Tyne, V. H., & Yakovina, L. A. 2004, *A&A*, 417, L39
- Pesic, D. S., Vujisic, B. R., Rakotoarijimy, D., & Weniger, S. 1983, *Journal of Molecular Spectroscopy*, 100, 245
- Peterson, R. C., Dalle Ore, C. M., & Kurucz, R. L. 1993, *ApJ*, 404, 333
- Phillips, J. G., & Davis, S. P. 1968, The Swan system of the C₂ molecule. The spectrum of the HgH molecule, ed. Phillips, J. G. & Davis, S. P.
- Rao, N. K., & Lambert, D. L. 2003, *PASP*, 115, 1304
- . 2008, *MNRAS*, 384, 477
- Rao, N. K., Sriram, S., Jayakumar, K., & Gabriel, F. 2005, *Journal of Astrophysics and Astronomy*, 26, 331
- Renzini, A. 1979, in *Astrophysics and Space Science Library*, Vol. 75, Stars and star systems, ed. B. E. Westerlund, 155–171
- Renzini, A. 1990, in *Astronomical Society of the Pacific Conference Series*, Vol. 11, Confrontation Between Stellar Pulsation and Evolution, ed. C. Cacciari & G. Clementini, 549–556
- Russo, R. E., Bol’Shakov, A. A., Mao, X., McKay, C. P., Perry, D. L., & Sorkhabi, O. 2011, *Spectrochimica Acta*, 66, 99
- Schmidt, T. W., & Bacskay, G. B. 2007, *J. Chem. Phys.*, 127, 234310
- Stawikowski, A., & Greenstein, J. L. 1964, *ApJ*, 140, 1280
- Tull, R. G., MacQueen, P. J., Sneden, C., & Lambert, D. L. 1995, *PASP*, 107, 251

Urdahl, R. S., Bao, Y., & Jackson, W. M. 1991, *Chemical Physics Letters*, 178, 425

Warner, B. 1967, *MNRAS*, 137, 119

Webbink, R. F. 1984, *ApJ*, 277, 355

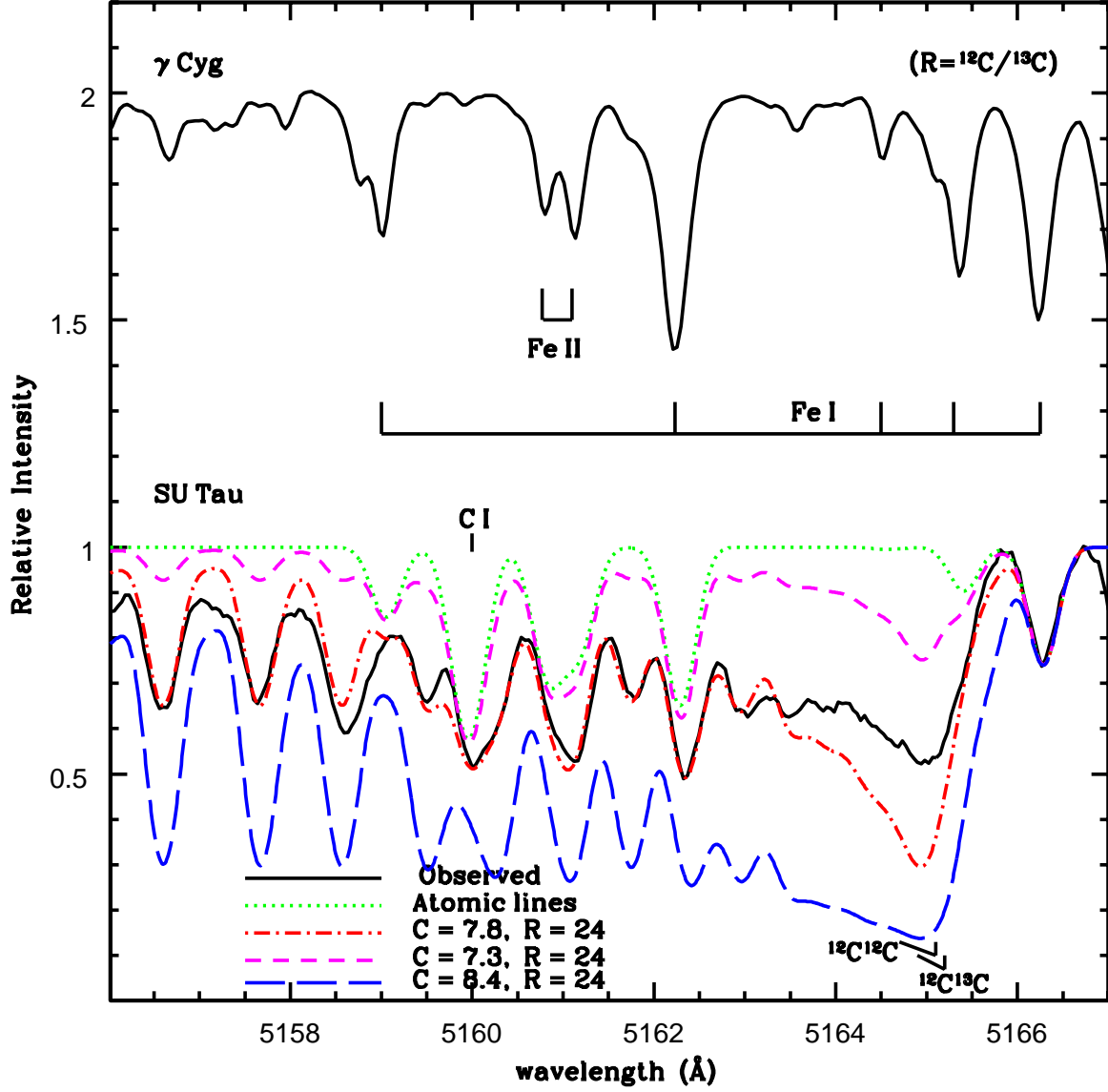


Fig. 1.— Observed and synthetic spectra of the (0,0) C_2 band for SU Tau. Synthetic spectra are plotted for different values of the C abundance – see key on the figure. The spectrum of the γ Cyg is plotted with the positions of the key lines marked.

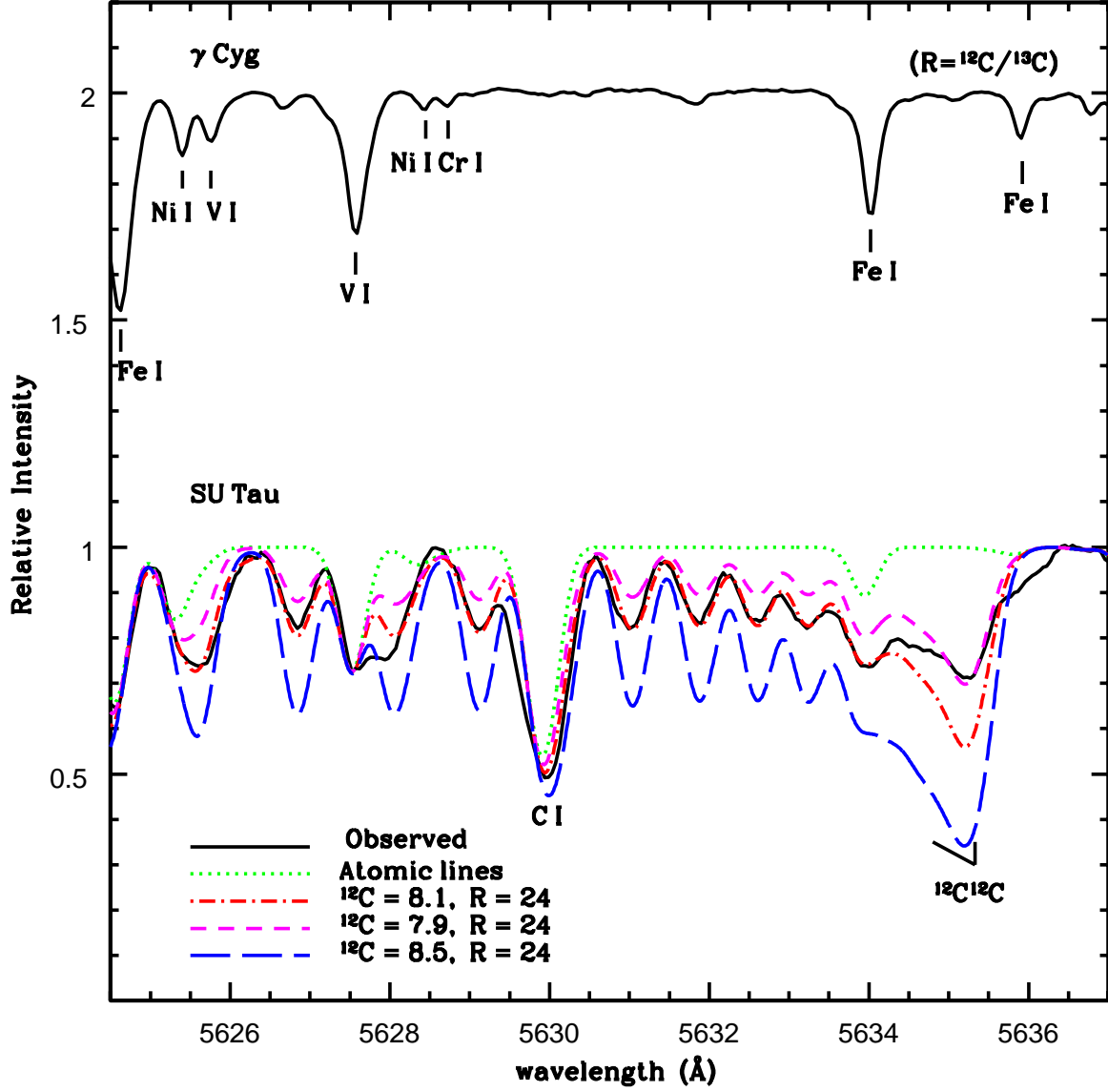


Fig. 2.— Observed and synthetic spectra of the (0,1) C_2 band for SU Tau. Synthetic spectra are plotted for different values of the C abundance – see key on the figure. The spectrum of the γ Cyg is plotted with the positions of the key lines marked.

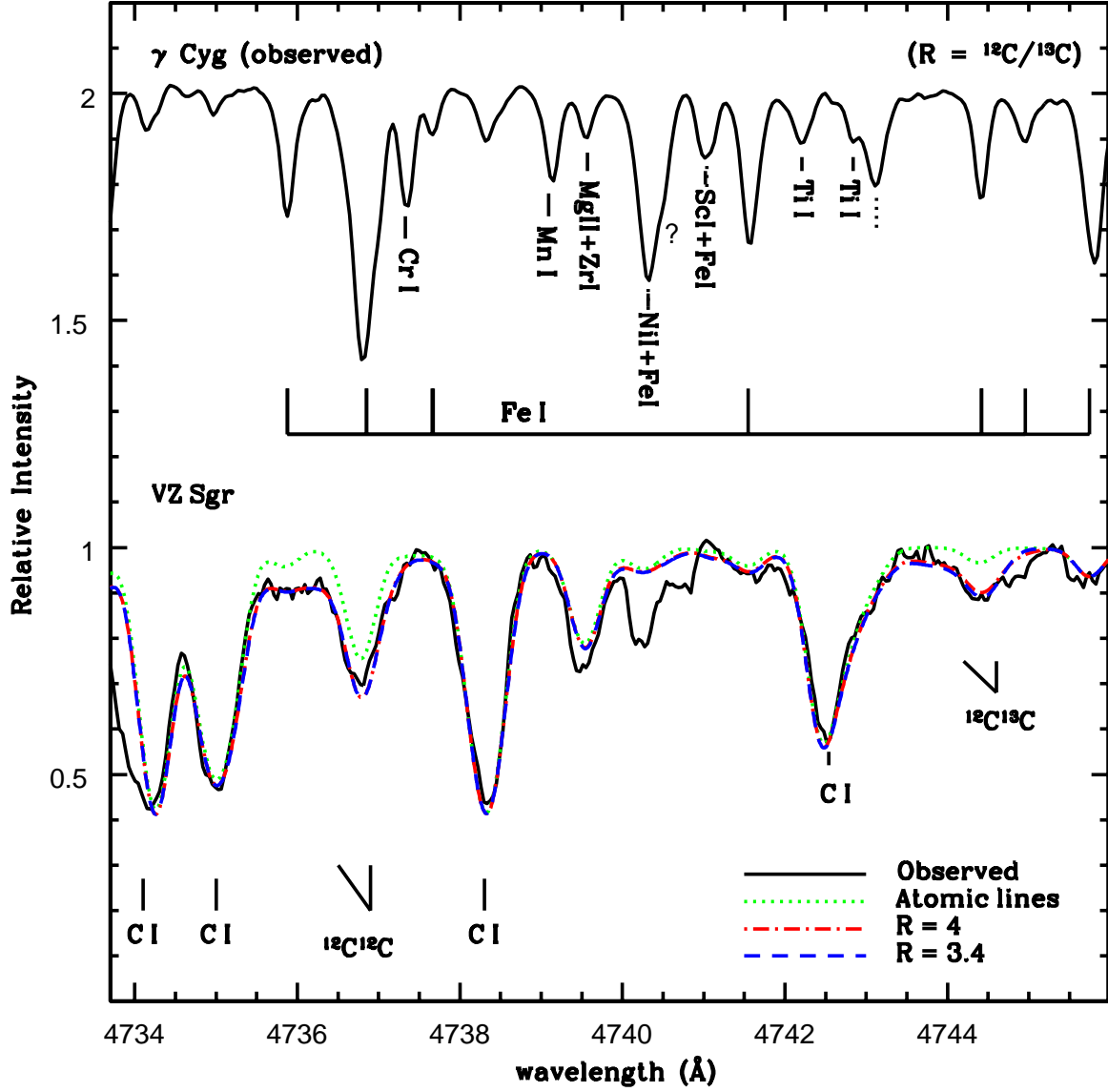


Fig. 3.— Observed and synthetic spectra of the (1,0) C_2 bands for VZ Sgr. Synthetic spectra are plotted for the values of the isotopic ratios (R) shown in the keys and for a spectrum with just the atomic lines. The spectrum of γ Cyg is also plotted – the positions of the key lines are also marked – the dotted line represents the blending of the one or more atomic lines.

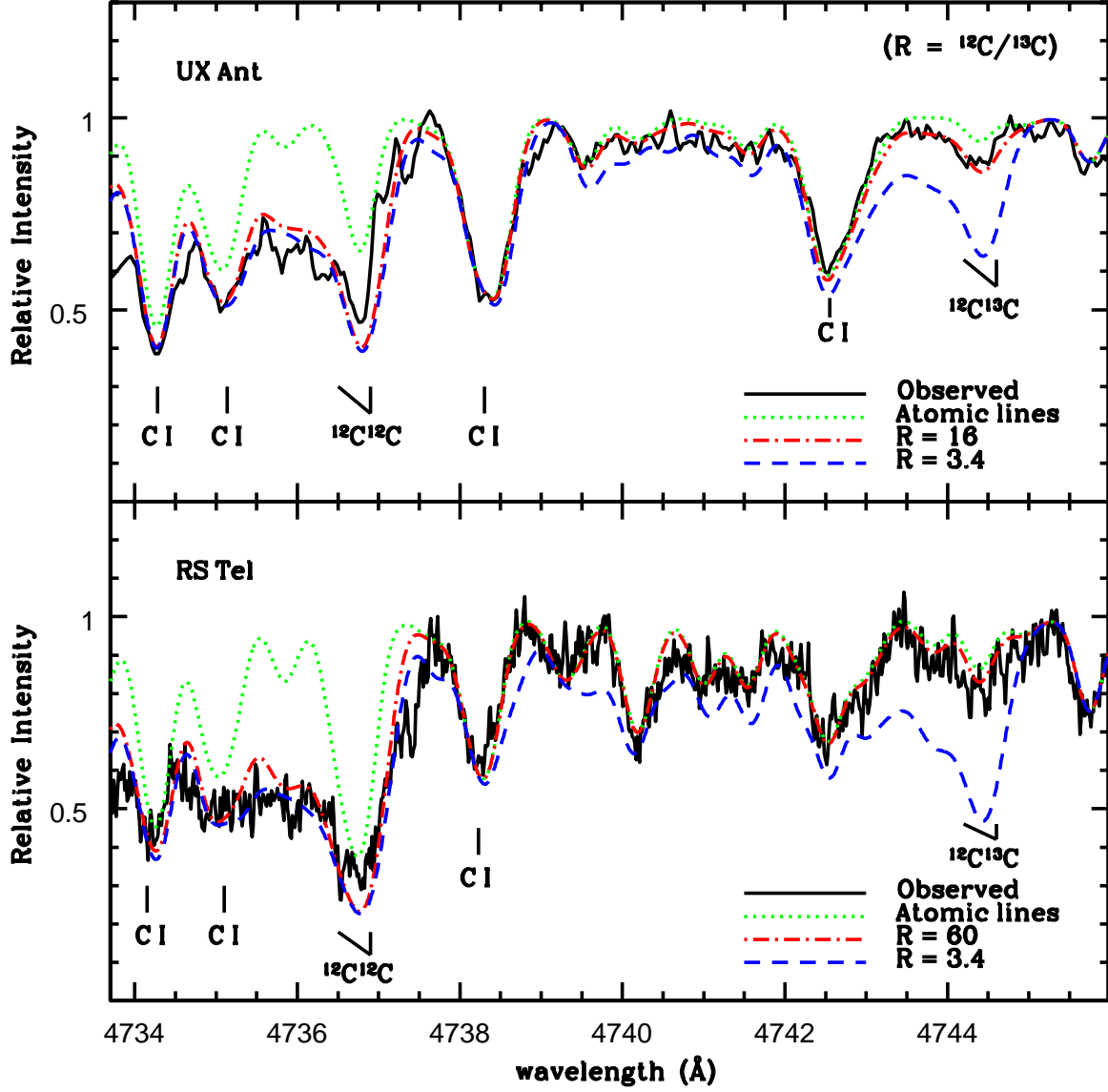


Fig. 4.— Observed and synthetic spectra of the (1,0) C_2 bands for UX Ant and RS Tel. Synthetic spectra are plotted for the values of the isotopic ratios (R) shown in the keys and for a spectrum with just the atomic lines. The positions of the key lines are also marked.

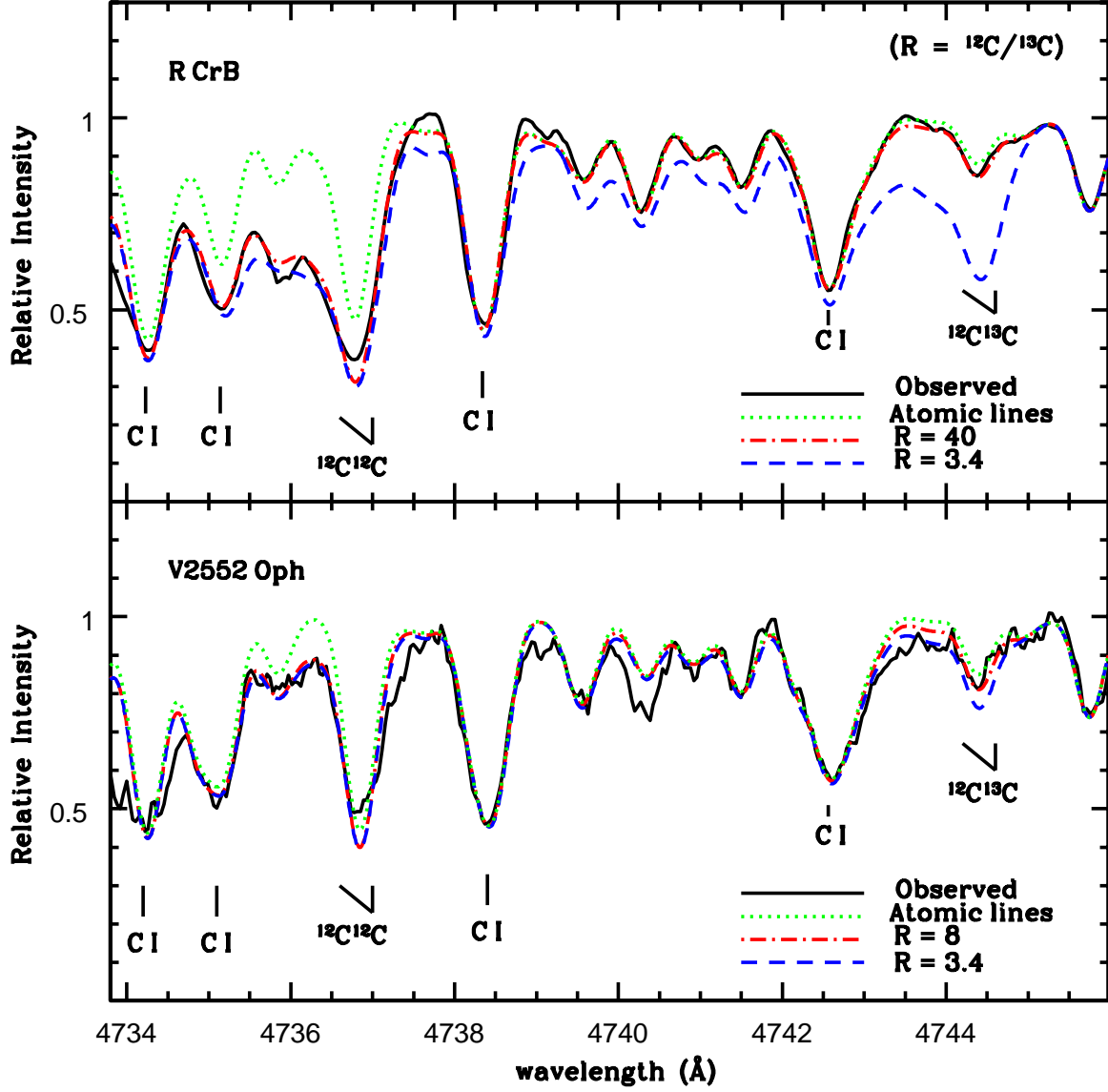


Fig. 5.— Observed and synthetic spectra of the (1,0) C_2 bands for R CrB and V2552 Oph. Synthetic spectra are plotted for the values of the isotopic ratios (R) shown in the keys and for a spectrum with just the atomic lines. The positions of the key lines are also marked.

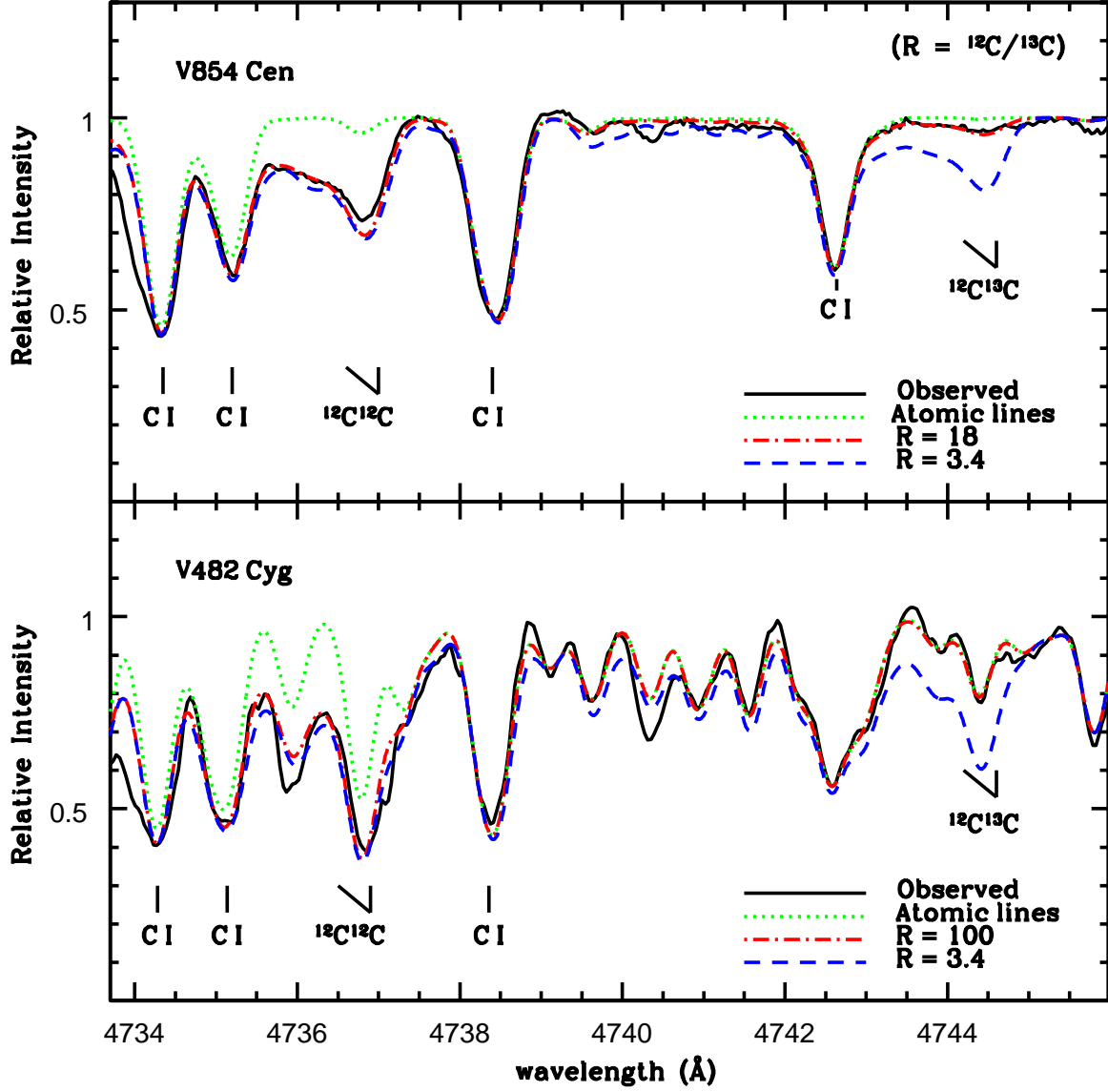


Fig. 6.— Observed and synthetic spectra of the (1,0) C₂ bands for V854Cen and V482 Cyg. Synthetic spectra are plotted for the values of the isotopic ratios (R) shown in the keys and for a spectrum with just the atomic lines. The positions of the key lines are also marked.

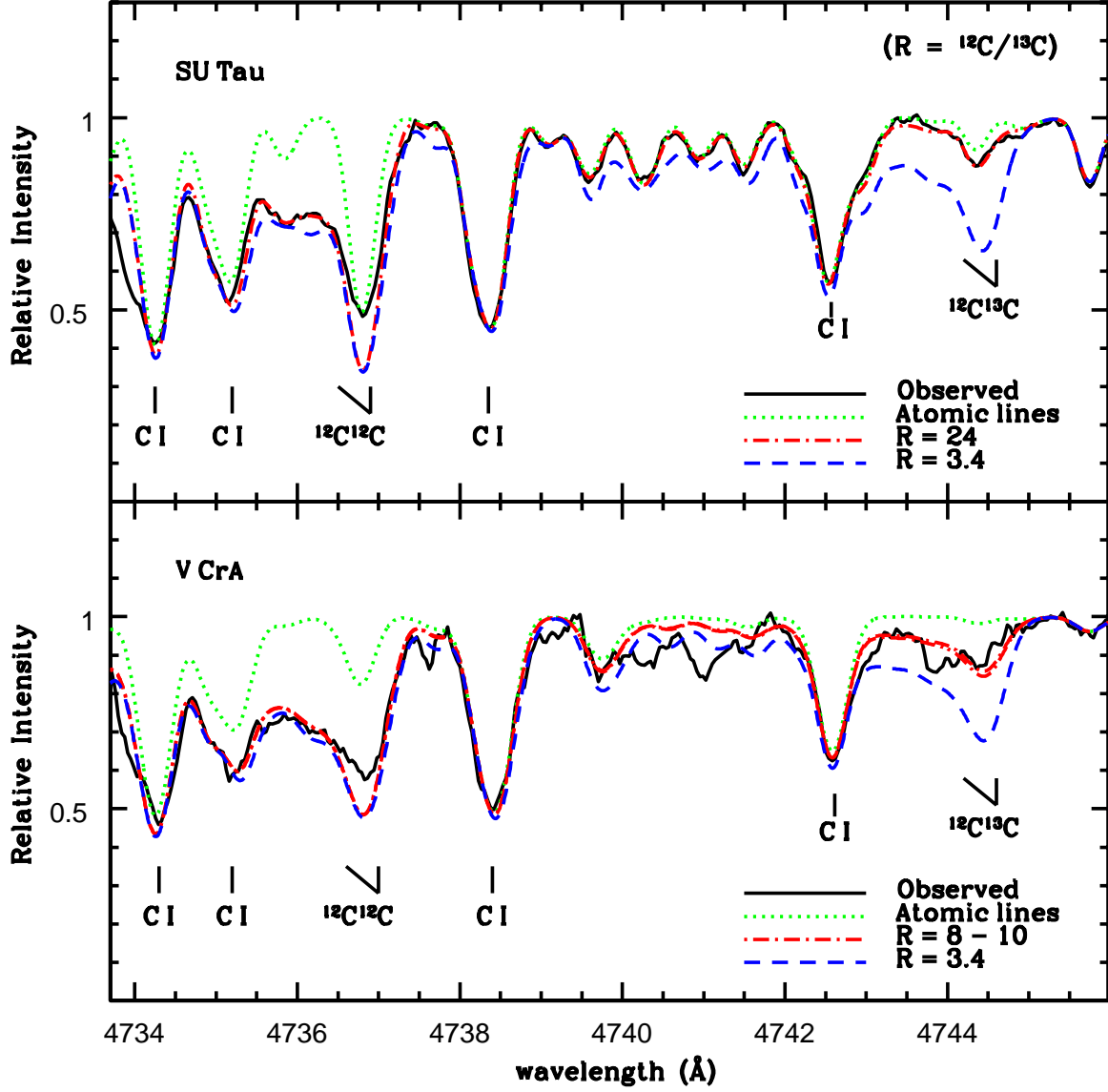


Fig. 7.— Observed and synthetic spectra of the (1,0) C_2 bands for SU Tau and V CrA. Synthetic spectra are plotted for the values of the isotopic ratios (R) shown in the keys and for a spectrum with just the atomic lines. The positions of the key lines are also marked.

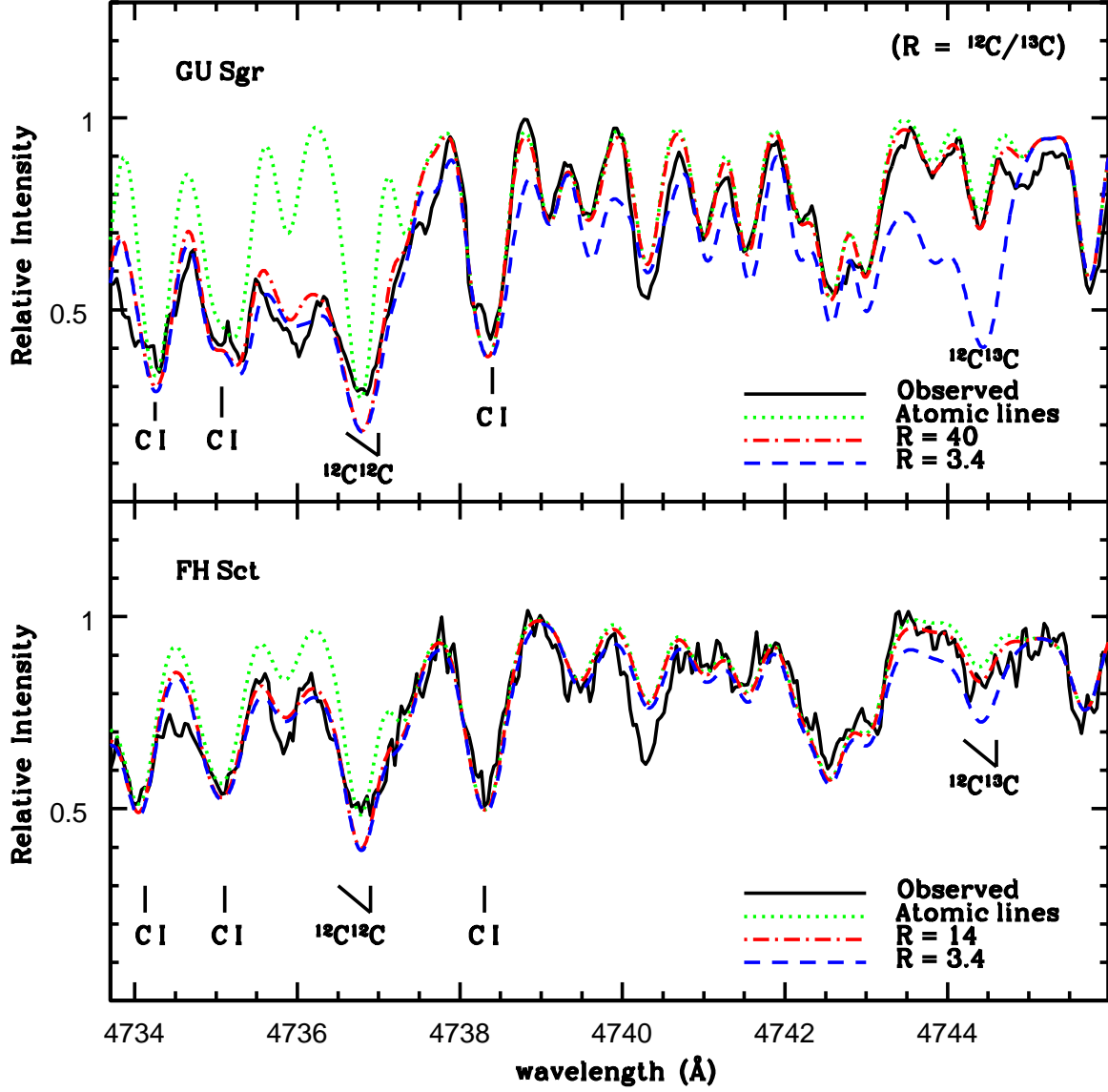


Fig. 8.— Observed and synthetic spectra of the (1,0) C_2 bands for GU Sgr and FH Sct. Synthetic spectra are plotted for the values of the isotopic ratios (R) shown in the keys and for a spectrum with just the atomic lines. The positions of the key lines are also marked.

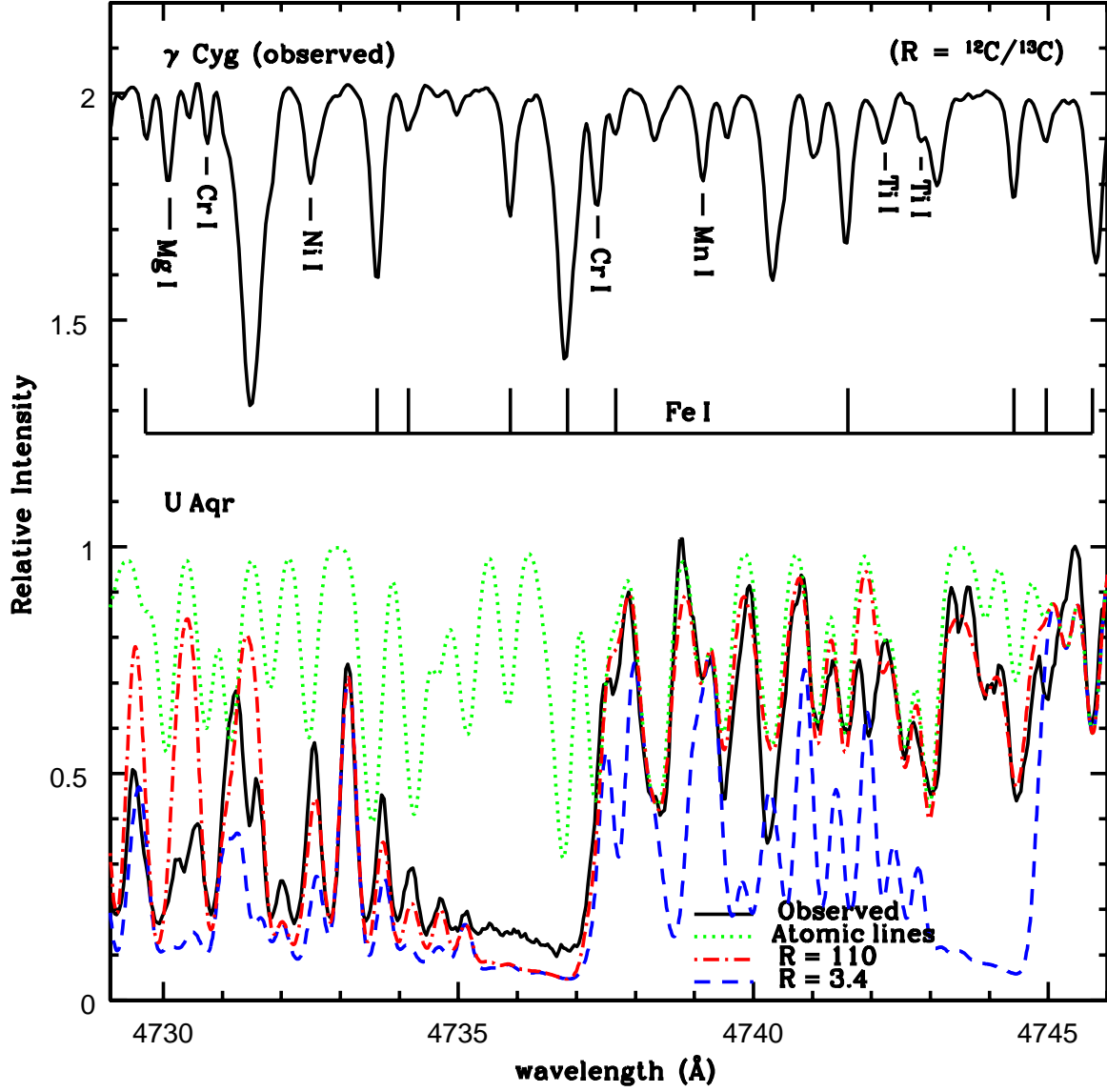


Fig. 9.— Observed and synthetic spectra of the (1,0) C_2 bands for U Aqr. Synthetic spectra are plotted for the values of the isotopic ratios (R) shown in the keys and for a spectrum with just the atomic lines. The spectrum of γ Cyg is also plotted – the positions of the key lines are also marked.

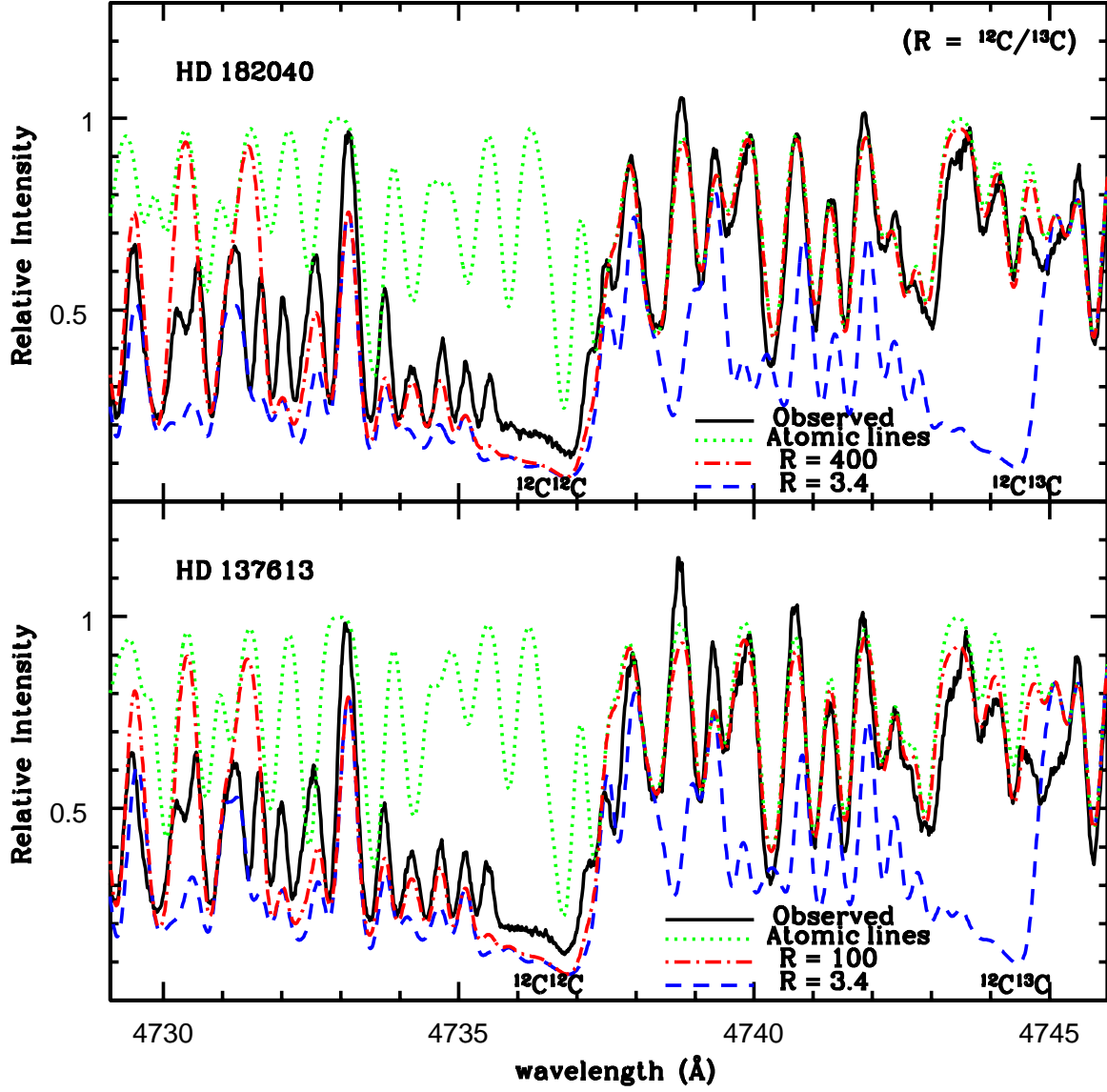


Fig. 10.— Observed and synthetic spectra of the (1,0) C₂ bands for HD 182040 and HD 137613. Synthetic spectra are plotted for the values of the isotopic ratios (R) shown in the keys and for a spectrum with just the atomic lines. The positions of the key lines are also marked.

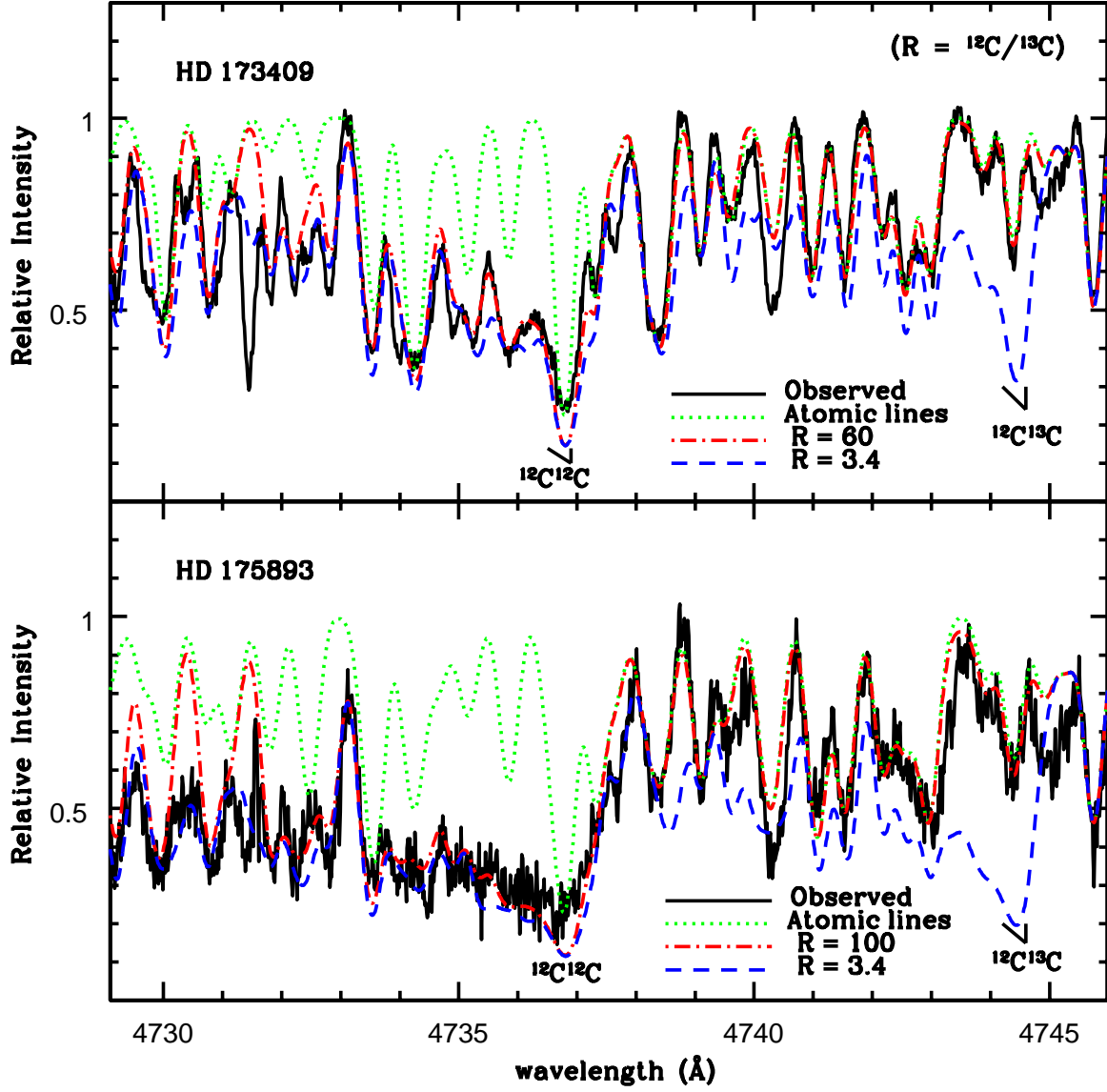


Fig. 11.— Observed and synthetic spectra of the (1,0) C_2 bands for HD 173409 and HD 175893. Synthetic spectra are plotted for the values of the isotopic ratios (R) shown in the keys and for a spectrum with just the atomic lines. The positions of the key lines are also marked.

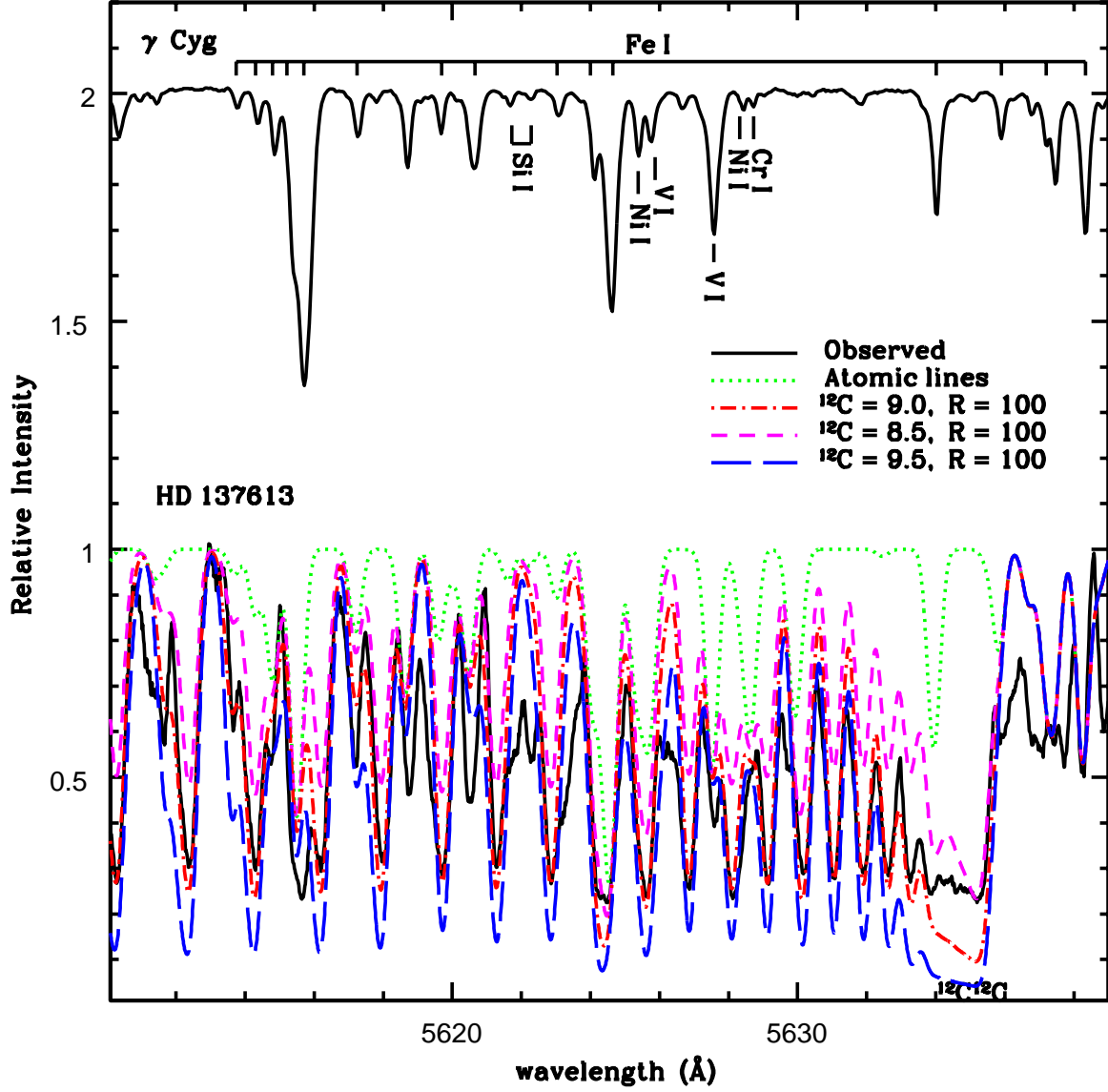


Fig. 12.— Observed and synthetic spectra of the (0,1) C₂ band for HD 137613. Synthetic spectra are plotted for different values of the C abundance – see key on the figure. The spectrum of the γ Cyg is plotted with the positions of the key lines marked.

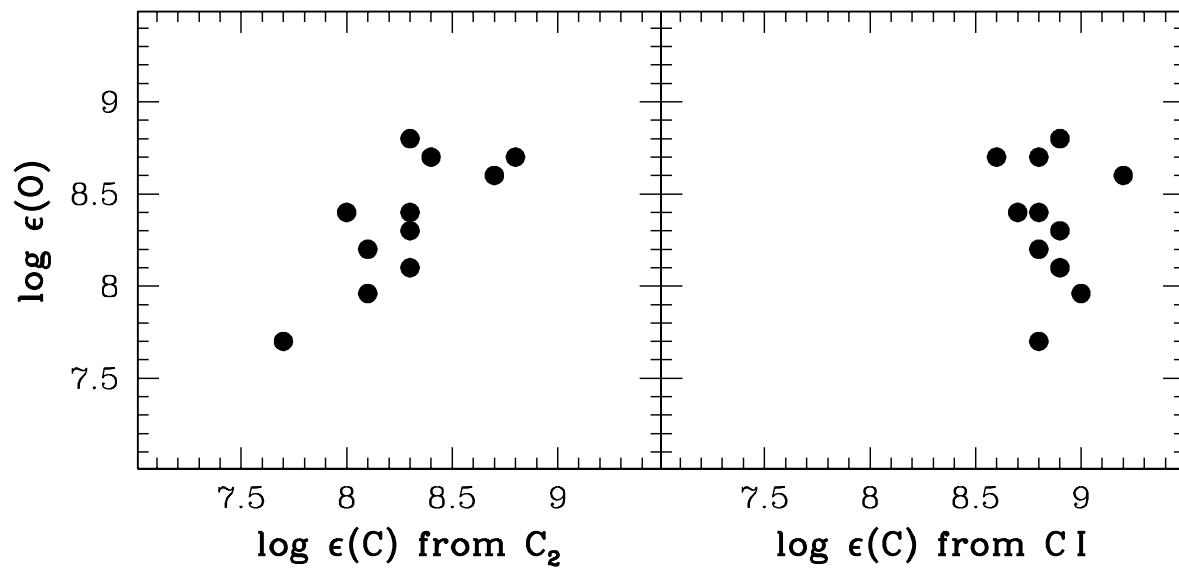


Fig. 13.— The plot of $\log \epsilon(\text{C})$, from C_2 bands and C I lines versus $\log \epsilon(\text{O})$ for RCB stars. The $\log \epsilon(\text{O})$ and the $\log \epsilon(\text{C})$, from C I lines, are from Asplund et al. (2000).

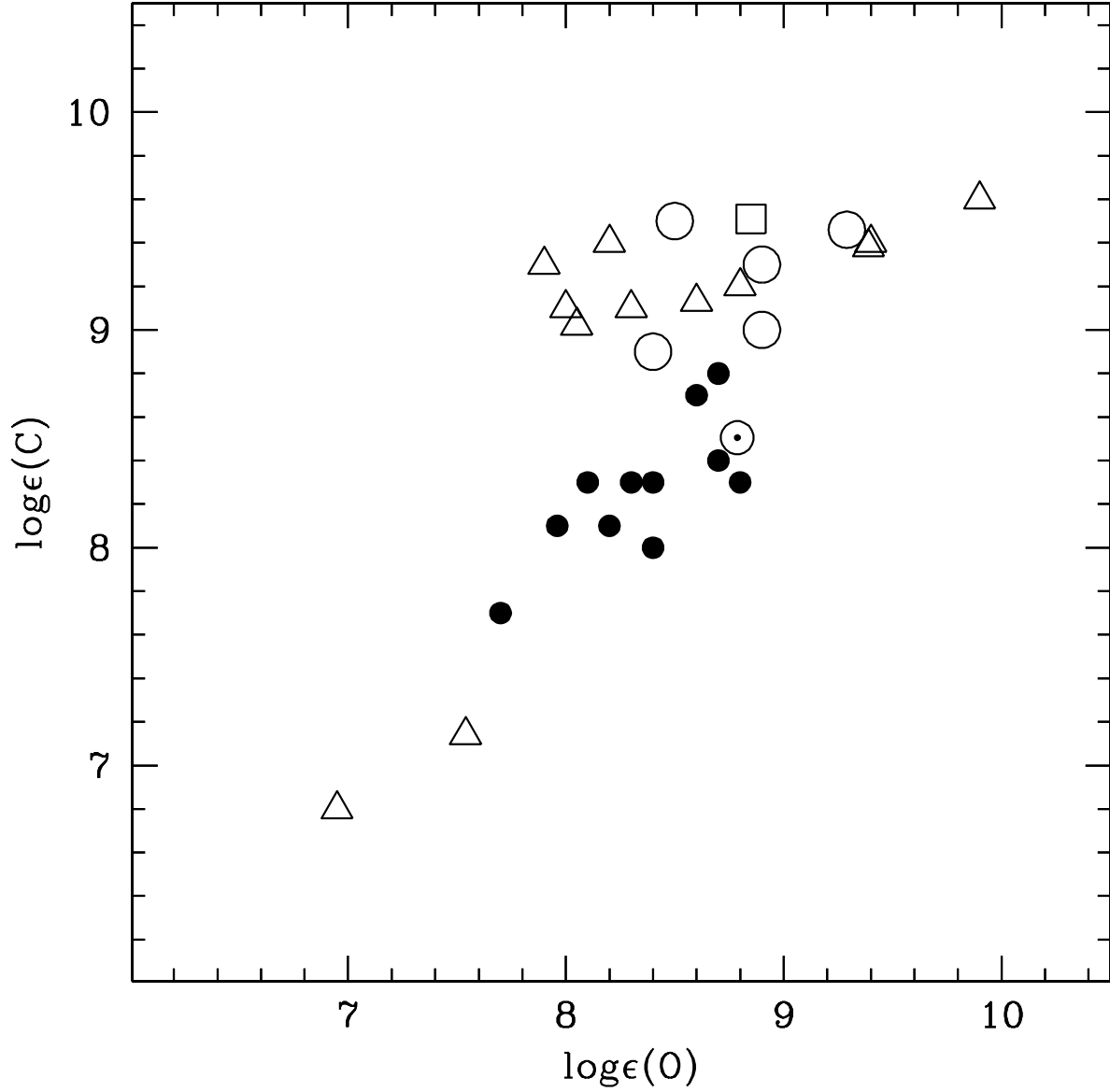


Fig. 14.— The plot of $\log \epsilon(\text{C})$ from C_2 bands versus $\log \epsilon(\text{O})$ (Asplund et al. 2000) for RCB stars. Also shown are the EHe stars. Our sample of eleven RCBs are represented by filled circles. Five cool EHes are represented by open circles (Pandey et al. 2001, 2006; Pandey & Reddy 2006). Twelve hot EHes are represented by open triangles (Drilling et al. 1998; Harrison & Jeffery 1997; Jeffery et al. 1998, 1999; Pandey & Lambert 2011). DY Cen, the hot minority RCB (Jeffery & Heber 1993) is represented by open square. \odot represents the Sun.

Table 1: Log of the observations: the stars are listed in the decreasing order of their effective temperature from top to bottom.

Star	Date of Observation	V	Obervatory	S/N Ratio
V3795 Sgr	26 July 1996	11.2	McDonald	110
XX Cam	17 November 2002	7.4	McDonald	200
VZ Sgr	22 May 2007	10.2	McDonald	200
UX Ant	5 May 2007	12.8	McDonald	120
RS Tel	28/29 May 2010	9.9	VB T	25
R CrB	5 May 2007	6.0	McDonald	200
V2552 Oph	22 May 2007	11.0	McDonald	128
V854 Cen	24-27 May 2010/10 February 1999	7.25	VB T/McDonald	250
V482 Cyg	23/24 May 2007	10.8	McDonald	152
SU Tau	15 Nov 2002	9.8	McDonald	196
V CrA	6 September 2003	9.5	McDonald	137
GU Sgr	23 May 2007	11.1	McDonald	135
FH Sct	24 May 2007	12.1	McDonald	87
U Aqr	23 July 1996	11.2	McDonald	125
HD 173409	27 May 2010	9.5	VB T	70
HD 182040	25 May 2010	7.0	VB T	110
HD 175893	25 May 2010	9.3	VB T	30
HD 137613	24 May 2010	7.5	VB T	90

Table 2. Molecular line list for the (1,0) C₂ swan band - ¹²C¹²C lines

Wavelength (Å)	J''	χ (eV)	$\log gf$
4692.348	28.0	0.342	-0.270
4692.485	28.0	0.342	-0.270
4692.548	27.0	0.342	-0.286
4692.679	26.0	0.342	-0.302
4692.794	61.0	0.940	0.064
4692.838	61.0	0.940	0.064
4692.848	62.0	0.940	0.071
4692.931	60.0	0.940	0.057
4693.077	60.0	0.940	0.057
4694.391	27.0	0.331	-0.286
4694.458	26.0	0.331	-0.302
4694.576	25.0	0.331	-0.319
4694.679	60.0	0.917	0.057
4694.687	61.0	0.917	0.064
4694.810	60.0	0.917	0.057
4696.325	26.0	0.321	-0.302
4696.386	25.0	0.321	-0.319
4696.520	24.0	0.321	-0.336
4696.593	59.0	0.893	0.049
4696.637	59.0	0.893	0.049
4696.643	60.0	0.893	0.057

Table 2—Continued

Wavelength (Å)	J''	χ (eV)	$\log gf$
4698.138	25.0	0.311	-0.319
4698.285	59.0	0.870	0.049
4698.292	57.0	0.870	0.034
4698.297	58.0	0.870	0.042
4698.339	23.0	0.311	-0.354
4698.406	57.0	0.870	0.034
4699.994	24.0	0.301	-0.336
4700.067	23.0	0.301	-0.354
4700.212	22.0	0.301	-0.373
4700.331	56.0	0.847	0.027
4701.729	23.0	0.292	-0.354
4701.817	22.0	0.292	-0.373
4701.841	56.0	0.825	0.027
4701.848	57.0	0.825	0.034
4701.942	21.0	0.292	-0.393
4701.962	55.0	0.825	0.019
4703.494	22.0	0.283	-0.373
4703.573	21.0	0.283	-0.393
4703.712	55.0	0.803	0.019
4703.728	20.0	0.283	-0.413
4703.732	55.0	0.803	0.019

Table 2—Continued

Wavelength (Å)	J''	χ (eV)	$\log gf$
4703.744	56.0	0.803	0.027
4703.815	54.0	0.803	0.011
4705.139	21.0	0.274	-0.393
4705.240	55.0	0.781	0.019
4705.250	20.0	0.275	-0.413
4705.272	54.0	0.781	0.011
4705.276	53.0	0.781	0.003
4705.339	53.0	0.781	0.003
4705.386	19.0	0.275	-0.435
4706.815	20.0	0.266	-0.413
4706.926	19.0	0.267	-0.435
4707.023	53.0	0.760	0.003
4707.039	53.0	0.760	0.003
4707.044	54.0	0.760	0.011
4707.079	18.0	0.267	-0.458
4707.135	52.0	0.760	-0.005
4708.383	19.0	0.259	-0.435
4708.474	52.0	0.739	-0.005
4708.483	53.0	0.739	0.003
4708.487	51.0	0.739	-0.013
4708.510	18.0	0.259	-0.458

Table 2—Continued

Wavelength (Å)	J''	χ (eV)	$\log gf$
4708.561	51.0	0.739	-0.013
4708.659	17.0	0.259	-0.482
4709.972	18.0	0.251	-0.458
4710.098	17.0	0.252	-0.482
4710.169	51.0	0.718	-0.013
4710.171	51.0	0.718	-0.013
4710.183	52.0	0.718	-0.005
4710.267	16.0	0.252	-0.508
4710.270	50.0	0.719	-0.022
4711.456	17.0	0.245	-0.482
4711.540	51.0	0.698	-0.013
4711.545	50.0	0.699	-0.022
4711.567	49.0	0.699	-0.031
4711.608	16.0	0.245	-0.508
4711.637	49.0	0.699	-0.031
4711.765	15.0	0.245	-0.535
4712.950	16.0	0.238	-0.508
4713.096	15.0	0.238	-0.535
4713.154	49.0	0.679	-0.031
4713.164	49.0	0.679	-0.031
4713.168	50.0	0.679	-0.022

Table 2—Continued

Wavelength (Å)	J''	χ (eV)	$\log gf$
4713.245	48.0	0.679	-0.039
4713.287	14.0	0.239	-0.564
4714.351	15.0	0.232	-0.535
4714.445	49.0	0.659	-0.031
4714.447	48.0	0.659	-0.039
4714.479	47.0	0.659	-0.049
4714.533	47.0	0.659	-0.049
4714.533	14.0	0.233	-0.564
4714.701	13.0	0.233	-0.595
4715.754	14.0	0.226	-0.564
4715.941	13.0	0.227	-0.595
4715.945	47.0	0.640	-0.049
4715.959	48.0	0.640	-0.039
4715.966	47.0	0.640	-0.049
4716.060	46.0	0.640	-0.058
4716.145	12.0	0.227	-0.628
4717.077	13.0	0.221	-0.595
4717.161	46.0	0.622	-0.058
4717.168	47.0	0.622	-0.049
4717.200	45.0	0.622	-0.067
4717.263	45.0	0.622	-0.067

Table 2—Continued

Wavelength (Å)	J''	χ (eV)	$\log gf$
4717.287	12.0	0.222	-0.628
4717.475	11.0	0.222	-0.665
4718.375	12.0	0.216	-0.628
4718.586	45.0	0.603	-0.067
4718.599	46.0	0.603	-0.058
4718.602	11.0	0.217	-0.665
4718.617	45.0	0.603	-0.067
4718.692	44.0	0.604	-0.077
4718.835	10.0	0.217	-0.704
4719.598	11.0	0.212	-0.665
4719.721	45.0	0.586	-0.067
4719.723	44.0	0.586	-0.077
4719.772	43.0	0.586	-0.087
4719.807	43.0	0.586	-0.087
4719.872	10.0	0.212	-0.704
4720.086	9.0	0.213	-0.747
4720.803	10.0	0.208	-0.704
4721.027	43.0	0.568	-0.087
4721.039	44.0	0.568	-0.077
4721.070	43.0	0.568	-0.087
4721.096	9.0	0.208	-0.747

Table 2—Continued

Wavelength (Å)	J''	χ (eV)	$\log gf$
4721.154	42.0	0.568	-0.097
4721.340	42.0	0.568	-0.097
4721.363	8.0	0.209	-0.796
4721.945	9.0	0.204	-0.747
4722.080	43.0	0.551	-0.087
4722.102	42.0	0.551	-0.097
4722.164	41.0	0.551	-0.107
4722.209	41.0	0.551	-0.107
4722.279	8.0	0.205	-0.796
4722.500	7.0	0.202	-0.850
4722.532	7.0	0.205	-0.850
4723.042	8.0	0.201	-0.796
4723.360	41.0	0.534	-0.107
4723.378	42.0	0.534	-0.097
4723.423	41.0	0.534	-0.107
4723.438	7.0	0.202	-0.850
4723.448	40.0	0.535	-0.118
4724.081	7.0	0.198	-0.850
4724.318	40.0	0.518	-0.118
4724.322	41.0	0.518	-0.107
4724.395	39.0	0.518	-0.129

Table 2—Continued

Wavelength (Å)	J''	χ (eV)	$\log gf$
4724.420	39.0	0.518	-0.129
4725.461	39.0	0.502	-0.129
4725.478	40.0	0.502	-0.118
4725.539	39.0	0.502	-0.129
4725.564	38.0	0.502	-0.140
4725.579	5.0	0.196	-0.985
4726.270	39.0	0.487	-0.129
4726.271	38.0	0.487	-0.140
4726.310	37.0	0.487	-0.151
4726.363	37.0	0.487	-0.151
4726.521	38.0	0.487	-0.140
4727.419	38.0	0.472	-0.140
4727.440	37.0	0.472	-0.151
4727.488	36.0	0.472	-0.163
4727.498	37.0	0.472	-0.151
4728.183	37.0	0.457	-0.151
4728.228	36.0	0.457	-0.163
4728.296	35.0	0.457	-0.175
4728.333	35.0	0.457	-0.175
4729.189	36.0	0.442	-0.163
4729.198	35.0	0.443	-0.175

Table 2—Continued

Wavelength (Å)	J''	χ (eV)	$\log gf$
4729.257	34.0	0.443	-0.187
4729.817	35.0	0.429	-0.175
4729.875	34.0	0.429	-0.187
4729.997	33.0	0.429	-0.200
4730.758	34.0	0.415	-0.187
4730.767	33.0	0.415	-0.200
4730.871	32.0	0.415	-0.213
4731.795	33.0	0.402	-0.200
4731.817	32.0	0.402	-0.213
4731.895	31.0	0.402	-0.227
4732.158	32.0	0.389	-0.213
4732.170	31.0	0.389	-0.227
4732.277	30.0	0.389	-0.241
4732.783	31.0	0.377	-0.227
4732.809	30.0	0.377	-0.241
4732.902	29.0	0.377	-0.255
4733.375	30.0	0.365	-0.241
4733.407	29.0	0.365	-0.255
4733.515	28.0	0.365	-0.270
4733.897	29.0	0.353	-0.255
4733.933	28.0	0.353	-0.270

Table 2—Continued

Wavelength (Å)	J''	χ (eV)	$\log gf$
4733.939	5.0	0.196	-0.985
4734.029	27.0	0.353	-0.286
4734.426	28.0	0.342	-0.270
4734.447	27.0	0.342	-0.286
4734.556	26.0	0.342	-0.302
4734.848	27.0	0.331	-0.286
4734.894	26.0	0.331	-0.302
4734.912	7.0	0.202	-0.850
4734.913	8.0	0.201	-0.796
4734.983	25.0	0.331	-0.319
4735.255	9.0	0.204	-0.747
4735.289	26.0	0.321	-0.302
4735.320	25.0	0.321	-0.319
4735.335	8.0	0.205	-0.796
4735.435	24.0	0.321	-0.336
4735.437	7.0	0.205	-0.850
4735.624	25.0	0.311	-0.319
4735.624	10.0	0.208	-0.704
4735.669	24.0	0.311	-0.336
4735.708	9.0	0.208	-0.747
4735.762	23.0	0.311	-0.354

Table 2—Continued

Wavelength (Å)	J''	χ (eV)	$\log gf$
4735.801	8.0	0.209	-0.796
4735.937	11.0	0.212	-0.665
4735.970	24.0	0.301	-0.336
4735.999	23.0	0.301	-0.354
4736.025	10.0	0.212	-0.704
4736.119	22.0	0.301	-0.373
4736.130	9.0	0.213	-0.747
4736.210	23.0	0.292	-0.354
4736.216	12.0	0.216	-0.628
4736.269	22.0	0.292	-0.373
4736.283	11.0	0.217	-0.665
4736.367	21.0	0.292	-0.393
4736.421	10.0	0.217	-0.704
4736.431	13.0	0.221	-0.595
4736.463	22.0	0.283	-0.373
4736.511	21.0	0.283	-0.393
4736.527	12.0	0.222	-0.628
4736.621	21.0	0.274	-0.393
4736.622	20.0	0.283	-0.413
4736.630	14.0	0.226	-0.564
4736.634	11.0	0.222	-0.665

Table 2—Continued

Wavelength (Å)	J''	χ (eV)	$\log gf$
4736.680	20.0	0.275	-0.413
4736.699	13.0	0.227	-0.595
4736.760	15.0	0.232	-0.535
4736.781	20.0	0.266	-0.413
4736.784	19.0	0.275	-0.435
4736.829	19.0	0.267	-0.435
4736.830	12.0	0.227	-0.628
4736.840	14.0	0.233	-0.564
4736.846	19.0	0.259	-0.435
4736.862	16.0	0.238	-0.508
4736.891	17.0	0.245	-0.482
4736.909	18.0	0.251	-0.458
4736.916	18.0	0.259	-0.458
4736.927	15.0	0.238	-0.535
4736.944	13.0	0.233	-0.595
4736.947	18.0	0.267	-0.458
4736.961	17.0	0.252	-0.482
4736.971	16.0	0.245	-0.508
4737.020	17.0	0.259	-0.482
4737.051	14.0	0.239	-0.564
4737.071	15.0	0.245	-0.535

Table 2—Continued

Wavelength (Å)	J''	χ (eV)	$\log gf$
4737.087	16.0	0.252	-0.508

Table 3. Molecular line list for the (1,0) C₂ swan band - ¹²C¹³C lines

Wavelength (Å)	J''	χ (eV)	$\log gf$
4700.760	28.0	0.342	-0.270
4701.749	28.0	0.342	-0.270
4701.736	27.0	0.342	-0.286
4701.789	26.0	0.342	-0.302
4703.775	61.0	0.940	0.064
4702.031	61.0	0.940	0.064
4702.111	62.0	0.940	0.071
4702.041	60.0	0.940	0.057
4703.961	60.0	0.940	0.057
4703.586	27.0	0.331	-0.286
4703.575	26.0	0.331	-0.302
4703.621	25.0	0.331	-0.319
4703.796	60.0	0.917	0.057
4703.887	61.0	0.917	0.064
4705.702	60.0	0.917	0.057
4705.450	26.0	0.321	-0.302
4705.438	25.0	0.321	-0.319
4705.498	24.0	0.321	-0.336
4707.382	59.0	0.893	0.049
4705.694	59.0	0.893	0.049
4705.767	60.0	0.893	0.057

Table 3—Continued

Wavelength (Å)	J''	χ (eV)	$\log gf$
4707.197	25.0	0.311	-0.319
4707.348	59.0	0.870	0.049
4708.886	57.0	0.870	0.034
4707.280	58.0	0.870	0.042
4707.254	23.0	0.311	-0.354
4707.325	57.0	0.870	0.034
4708.985	24.0	0.301	-0.336
4708.989	23.0	0.301	-0.354
4709.064	22.0	0.301	-0.373
4709.182	56.0	0.847	0.027
4710.657	23.0	0.292	-0.354
4710.675	22.0	0.292	-0.373
4710.697	56.0	0.825	0.027
4710.780	57.0	0.825	0.034
4710.733	21.0	0.292	-0.393
4710.757	55.0	0.825	0.019
4712.358	22.0	0.283	-0.373
4712.371	21.0	0.283	-0.393
4714.134	55.0	0.803	0.019
4712.459	20.0	0.283	-0.413
4712.534	55.0	0.803	0.019

Table 3—Continued

Wavelength (Å)	J''	χ (eV)	$\log gf$
4712.607	56.0	0.803	0.027
4712.545	54.0	0.803	0.011
4713.942	21.0	0.274	-0.393
4714.047	55.0	0.781	0.019
4713.987	20.0	0.275	-0.413
4714.007	54.0	0.781	0.011
4715.515	53.0	0.781	0.003
4714.016	53.0	0.781	0.003
4714.060	19.0	0.275	-0.435
4715.558	20.0	0.266	-0.413
4715.605	19.0	0.267	-0.435
4717.270	53.0	0.760	0.003
4715.722	53.0	0.760	0.003
4715.786	54.0	0.760	0.011
4715.695	18.0	0.267	-0.458
4715.750	52.0	0.760	-0.005
4717.068	19.0	0.259	-0.435
4717.094	52.0	0.739	-0.005
4717.172	53.0	0.739	0.003
4718.557	51.0	0.739	-0.013
4717.132	18.0	0.259	-0.458

Table 3—Continued

Wavelength (Å)	J''	χ (eV)	$\log gf$
4717.126	51.0	0.739	-0.013
4717.221	17.0	0.259	-0.482
4718.599	18.0	0.251	-0.458
4718.665	17.0	0.252	-0.482
4720.246	51.0	0.718	-0.013
4718.742	51.0	0.718	-0.013
4718.809	52.0	0.718	-0.005
4718.775	16.0	0.252	-0.508
4718.777	50.0	0.719	-0.022
4720.028	17.0	0.245	-0.482
4720.116	51.0	0.698	-0.013
4720.056	50.0	0.699	-0.022
4721.474	49.0	0.699	-0.031
4720.121	16.0	0.245	-0.508
4720.096	49.0	0.699	-0.031
4720.221	15.0	0.245	-0.535
4721.468	16.0	0.238	-0.508
4721.557	15.0	0.238	-0.535
4721.618	49.0	0.679	-0.031
4723.078	49.0	0.679	-0.031
4721.685	50.0	0.679	-0.022

Table 3—Continued

Wavelength (Å)	J''	χ (eV)	$\log gf$
4721.649	48.0	0.679	-0.039
4721.692	14.0	0.239	-0.564
4722.817	15.0	0.232	-0.535
4722.914	49.0	0.659	-0.031
4722.855	48.0	0.659	-0.039
4724.229	47.0	0.659	-0.049
4722.892	47.0	0.659	-0.049
4722.943	14.0	0.233	-0.564
4723.058	13.0	0.233	-0.595
4724.168	14.0	0.226	-0.564
4724.302	13.0	0.227	-0.595
4724.309	47.0	0.640	-0.049
4724.373	48.0	0.640	-0.039
4725.722	47.0	0.640	-0.049
4724.367	46.0	0.640	-0.058
4724.454	12.0	0.227	-0.628
4725.442	13.0	0.221	-0.595
4725.472	46.0	0.622	-0.058
4725.536	47.0	0.622	-0.049
4726.799	45.0	0.622	-0.067
4725.528	45.0	0.622	-0.067

Table 3—Continued

Wavelength (Å)	J''	χ (eV)	$\log gf$
4725.600	12.0	0.222	-0.628
4725.738	11.0	0.222	-0.665
4726.692	12.0	0.216	-0.628
4726.856	45.0	0.603	-0.067
4726.915	46.0	0.603	-0.058
4726.869	11.0	0.217	-0.665
4728.222	45.0	0.603	-0.067
4726.909	44.0	0.604	-0.077
4727.054	10.0	0.217	-0.704
4727.869	11.0	0.212	-0.665
4727.995	45.0	0.586	-0.067
4727.944	44.0	0.586	-0.077
4729.226	43.0	0.586	-0.087
4727.985	43.0	0.586	-0.087
4728.094	10.0	0.212	-0.704
4728.262	9.0	0.213	-0.747
4729.029	10.0	0.208	-0.704
4729.209	43.0	0.568	-0.087
4729.264	44.0	0.568	-0.077
4730.529	43.0	0.568	-0.087
4729.276	9.0	0.208	-0.747

Table 3—Continued

Wavelength (Å)	J''	χ (eV)	$\log gf$
4729.287	42.0	0.568	-0.097
4730.728	42.0	0.568	-0.097
4729.498	8.0	0.209	-0.796
4730.128	9.0	0.204	-0.747
4730.265	43.0	0.551	-0.087
4730.238	42.0	0.551	-0.097
4731.478	41.0	0.551	-0.107
4730.305	41.0	0.551	-0.107
4730.417	8.0	0.205	-0.796
4730.357	7.0	0.202	-0.850
4730.627	7.0	0.205	-0.850
4731.183	8.0	0.201	-0.796
4731.460	41.0	0.534	-0.107
4731.519	42.0	0.534	-0.097
4732.742	41.0	0.534	-0.107
4731.536	7.0	0.202	-0.850
4731.503	40.0	0.535	-0.118
4732.181	7.0	0.198	-0.850
4732.376	40.0	0.518	-0.118
4732.426	41.0	0.518	-0.107
4733.576	39.0	0.518	-0.129

Table 3—Continued

Wavelength (Å)	J''	χ (eV)	$\log gf$
4732.441	39.0	0.518	-0.129
4733.486	39.0	0.502	-0.129
4733.540	40.0	0.502	-0.118
4734.724	39.0	0.502	-0.129
4733.548	38.0	0.502	-0.140
4733.602	5.0	0.196	-0.985
4734.298	39.0	0.487	-0.129
4734.257	38.0	0.487	-0.140
4734.262	37.0	0.487	-0.151
4735.417	37.0	0.487	-0.151
4735.645	38.0	0.487	-0.140
4735.409	38.0	0.472	-0.140
4735.396	37.0	0.472	-0.151
4735.406	36.0	0.472	-0.163
4736.556	37.0	0.472	-0.151
4736.141	37.0	0.457	-0.151
4736.149	36.0	0.457	-0.163
4736.186	35.0	0.457	-0.175
4737.266	35.0	0.457	-0.175
4737.113	36.0	0.442	-0.163
4737.091	35.0	0.443	-0.175

Table 3—Continued

Wavelength (Å)	J''	χ (eV)	$\log gf$
4737.116	34.0	0.443	-0.187
4737.712	35.0	0.429	-0.175
4737.736	34.0	0.429	-0.187
4738.815	33.0	0.429	-0.200
4738.622	34.0	0.415	-0.187
4738.603	33.0	0.415	-0.200
4738.678	32.0	0.415	-0.213
4739.635	33.0	0.402	-0.200
4739.627	32.0	0.402	-0.213
4739.681	31.0	0.402	-0.227
4739.969	32.0	0.389	-0.213
4739.956	31.0	0.389	-0.227
4740.037	30.0	0.389	-0.241
4740.571	31.0	0.377	-0.227
4740.571	30.0	0.377	-0.241
4740.643	29.0	0.377	-0.255
4741.139	30.0	0.365	-0.241
4741.150	29.0	0.365	-0.255
4741.235	28.0	0.365	-0.270
4741.641	29.0	0.353	-0.255
4741.655	28.0	0.353	-0.270

Table 3—Continued

Wavelength (Å)	J''	χ (eV)	$\log gf$
4741.661	5.0	0.196	-0.985
4741.733	27.0	0.353	-0.286
4742.149	28.0	0.342	-0.270
4742.153	27.0	0.342	-0.286
4742.243	26.0	0.342	-0.302
4742.555	27.0	0.331	-0.286
4742.582	26.0	0.331	-0.302
4742.600	7.0	0.202	-0.850
4742.586	8.0	0.201	-0.796
4742.657	25.0	0.331	-0.319
4742.915	9.0	0.204	-0.747
4742.978	26.0	0.321	-0.302
4742.995	25.0	0.321	-0.319
4743.009	8.0	0.205	-0.796
4743.095	24.0	0.321	-0.336
4743.127	7.0	0.205	-0.850
4743.300	25.0	0.311	-0.319
4743.272	10.0	0.208	-0.704
4743.330	24.0	0.311	-0.336
4743.369	9.0	0.208	-0.747
4743.412	23.0	0.311	-0.354

Table 3—Continued

Wavelength (Å)	J''	χ (eV)	$\log gf$
4743.476	8.0	0.209	-0.796
4743.576	11.0	0.212	-0.665
4743.632	24.0	0.301	-0.336
4743.649	23.0	0.301	-0.354
4743.675	10.0	0.212	-0.704
4743.758	22.0	0.301	-0.373
4743.793	9.0	0.213	-0.747
4743.861	23.0	0.292	-0.354
4743.847	12.0	0.216	-0.628
4743.909	22.0	0.292	-0.373
4743.923	11.0	0.217	-0.665
4743.999	21.0	0.292	-0.393
4744.072	10.0	0.217	-0.704
4744.056	13.0	0.221	-0.595
4744.103	22.0	0.283	-0.373
4744.144	21.0	0.283	-0.393
4744.159	12.0	0.222	-0.628
4744.254	21.0	0.274	-0.393
4744.247	20.0	0.283	-0.413
4744.250	14.0	0.226	-0.564
4744.275	11.0	0.222	-0.665

Table 3—Continued

Wavelength (Å)	J''	χ (eV)	$\log gf$
4744.305	20.0	0.275	-0.413
4744.325	13.0	0.227	-0.595
4744.377	15.0	0.232	-0.535
4744.407	20.0	0.266	-0.413
4744.405	19.0	0.275	-0.435
4744.450	19.0	0.267	-0.435
4744.463	12.0	0.227	-0.628
4744.461	14.0	0.233	-0.564
4744.467	19.0	0.259	-0.435
4744.477	16.0	0.238	-0.508
4744.507	17.0	0.245	-0.482
4744.526	18.0	0.251	-0.458
4744.533	18.0	0.259	-0.458
4744.545	15.0	0.238	-0.535
4744.570	13.0	0.233	-0.595
4744.564	18.0	0.267	-0.458
4744.577	17.0	0.252	-0.482
4744.587	16.0	0.245	-0.508
4744.636	17.0	0.259	-0.482
4744.672	14.0	0.239	-0.564
4744.689	15.0	0.245	-0.535

Table 3—Continued

Wavelength (Å)	J''	χ (eV)	$\log gf$
4744.703	16.0	0.252	-0.508

Table 4. Molecular line list for the (0,0) C₂ swan band - ¹²C¹²C lines

Wavelength (Å)	J''	χ (eV)	$\log gf$
5129.601	47.0	0.640	0.465
5129.601	48.0	0.640	0.474
5129.601	47.0	0.640	0.465
5129.601	48.0	0.640	0.474
5129.694	46.0	0.640	0.455
5129.694	46.0	0.640	0.455
5130.272	19.0	0.259	0.078
5130.418	18.0	0.259	0.055
5130.583	17.0	0.259	0.031
5131.584	47.0	0.622	0.465
5131.584	46.0	0.622	0.455
5131.584	47.0	0.622	0.465
5131.584	46.0	0.622	0.455
5131.699	45.0	0.622	0.446
5131.699	45.0	0.622	0.446
5132.360	18.0	0.251	0.055
5132.497	17.0	0.252	0.031
5132.699	16.0	0.252	0.006
5133.719	46.0	0.603	0.455
5133.719	45.0	0.603	0.446
5133.719	46.0	0.603	0.455

Table 4—Continued

Wavelength (Å)	J''	χ (eV)	$\log gf$
5133.719	45.0	0.603	0.446
5133.825	44.0	0.604	0.436
5133.825	44.0	0.604	0.436
5134.319	17.0	0.245	0.031
5134.489	16.0	0.245	0.006
5134.671	15.0	0.245	-0.022
5135.586	44.0	0.586	0.436
5135.586	45.0	0.586	0.446
5135.586	45.0	0.586	0.446
5135.586	44.0	0.586	0.436
5135.693	43.0	0.586	0.427
5135.693	43.0	0.586	0.427
5136.274	16.0	0.238	0.006
5136.440	15.0	0.238	-0.022
5136.660	14.0	0.239	-0.051
5137.586	44.0	0.568	0.436
5137.586	43.0	0.568	0.427
5137.586	44.0	0.568	0.436
5137.586	43.0	0.568	0.427
5137.696	42.0	0.568	0.416
5137.696	42.0	0.568	0.416

Table 4—Continued

Wavelength (Å)	J''	χ (eV)	$\log gf$
5138.112	15.0	0.232	-0.022
5138.316	14.0	0.233	-0.051
5138.510	13.0	0.233	-0.082
5139.323	43.0	0.551	0.427
5139.323	42.0	0.551	0.416
5139.323	43.0	0.551	0.427
5139.323	42.0	0.551	0.416
5139.448	41.0	0.551	0.406
5139.448	41.0	0.551	0.406
5139.933	14.0	0.226	-0.051
5140.143	13.0	0.227	-0.082
5140.381	12.0	0.227	-0.115
5141.206	41.0	0.534	0.406
5141.206	41.0	0.534	0.406
5141.206	42.0	0.534	0.416
5141.206	42.0	0.534	0.416
5141.318	40.0	0.535	0.395
5141.318	40.0	0.535	0.395
5141.648	13.0	0.221	-0.082
5141.896	12.0	0.222	-0.115
5142.114	11.0	0.222	-0.151

Table 4—Continued

Wavelength (Å)	J''	χ (eV)	$\log gf$
5142.843	40.0	0.518	0.395
5142.843	41.0	0.518	0.406
5142.843	41.0	0.518	0.406
5142.843	40.0	0.518	0.395
5142.935	39.0	0.518	0.385
5142.935	39.0	0.518	0.385
5143.332	12.0	0.216	-0.115
5143.599	11.0	0.217	-0.151
5143.863	10.0	0.217	-0.191
5144.575	40.0	0.502	0.395
5144.575	39.0	0.502	0.385
5144.575	40.0	0.502	0.395
5144.575	39.0	0.502	0.385
5144.694	38.0	0.502	0.373
5144.694	38.0	0.502	0.373
5144.924	11.0	0.212	-0.151
5145.232	10.0	0.212	-0.191
5145.476	9.0	0.213	-0.234
5146.082	38.0	0.487	0.373
5146.082	39.0	0.487	0.385
5146.082	38.0	0.487	0.373

Table 4—Continued

Wavelength (Å)	J''	χ (eV)	$\log gf$
5146.082	39.0	0.487	0.385
5146.207	37.0	0.487	0.362
5146.207	37.0	0.487	0.362
5146.465	10.0	0.208	-0.191
5146.813	9.0	0.208	-0.234
5147.115	8.0	0.209	-0.283
5147.691	38.0	0.472	0.373
5147.691	38.0	0.472	0.373
5147.691	37.0	0.472	0.362
5147.691	37.0	0.472	0.362
5147.816	36.0	0.472	0.350
5147.816	36.0	0.472	0.350
5147.929	9.0	0.204	-0.234
5148.325	8.0	0.205	-0.283
5148.607	7.0	0.205	-0.337
5149.088	36.0	0.457	0.350
5149.088	36.0	0.457	0.350
5149.088	37.0	0.457	0.362
5149.088	37.0	0.457	0.362
5149.210	35.0	0.457	0.338
5149.210	35.0	0.457	0.338

Table 4—Continued

Wavelength (Å)	J''	χ (eV)	$\log gf$
5149.330	8.0	0.201	-0.283
5149.787	7.0	0.202	-0.337
5150.558	35.0	0.443	0.338
5150.558	36.0	0.442	0.350
5150.558	35.0	0.443	0.338
5150.558	36.0	0.442	0.350
5150.667	7.0	0.198	-0.337
5150.667	34.0	0.443	0.326
5150.667	34.0	0.443	0.326
5151.831	35.0	0.429	0.338
5151.831	35.0	0.429	0.338
5151.865	34.0	0.429	0.326
5151.865	34.0	0.429	0.326
5151.933	33.0	0.429	0.313
5151.933	33.0	0.429	0.313
5152.515	5.0	0.196	-0.472
5153.172	33.0	0.415	0.313
5153.172	33.0	0.415	0.313
5153.172	34.0	0.415	0.326
5153.172	34.0	0.415	0.326
5153.291	32.0	0.415	0.300

Table 4—Continued

Wavelength (Å)	J''	χ (eV)	$\log gf$
5153.291	32.0	0.415	0.300
5154.337	32.0	0.402	0.300
5154.337	33.0	0.402	0.313
5154.337	33.0	0.402	0.313
5154.337	32.0	0.402	0.300
5154.452	31.0	0.402	0.286
5154.452	31.0	0.402	0.286
5155.516	32.0	0.389	0.300
5155.516	32.0	0.389	0.300
5155.524	31.0	0.389	0.286
5155.524	31.0	0.389	0.286
5155.649	30.0	0.389	0.272
5155.649	30.0	0.389	0.272
5156.537	31.0	0.377	0.286
5156.537	31.0	0.377	0.286
5156.587	30.0	0.377	0.272
5156.587	30.0	0.377	0.272
5156.686	29.0	0.377	0.258
5156.686	29.0	0.377	0.258
5157.605	30.0	0.365	0.272
5157.605	30.0	0.365	0.272

Table 4—Continued

Wavelength (Å)	J''	χ (eV)	$\log gf$
5157.643	29.0	0.365	0.258
5157.643	29.0	0.365	0.258
5157.758	28.0	0.365	0.243
5157.758	28.0	0.365	0.243
5158.490	29.0	0.353	0.258
5158.490	29.0	0.353	0.258
5158.562	28.0	0.353	0.243
5158.562	28.0	0.353	0.243
5158.654	27.0	0.353	0.227
5158.654	27.0	0.353	0.227
5159.453	28.0	0.342	0.243
5159.453	28.0	0.342	0.243
5159.470	27.0	0.342	0.227
5159.470	27.0	0.342	0.227
5159.600	26.0	0.342	0.211
5159.600	26.0	0.342	0.211
5160.213	27.0	0.331	0.227
5160.213	27.0	0.331	0.227
5160.283	26.0	0.331	0.211
5160.283	26.0	0.331	0.211
5160.385	25.0	0.331	0.195

Table 4—Continued

Wavelength (Å)	J''	χ (eV)	$\log gf$
5160.385	25.0	0.331	0.195
5161.037	26.0	0.321	0.211
5161.037	26.0	0.321	0.211
5161.054	25.0	0.321	0.195
5161.054	25.0	0.321	0.195
5161.188	24.0	0.321	0.177
5161.188	24.0	0.321	0.177
5161.680	25.0	0.311	0.195
5161.680	25.0	0.311	0.195
5161.741	24.0	0.311	0.177
5161.741	24.0	0.311	0.177
5161.854	23.0	0.311	0.159
5161.854	23.0	0.311	0.159
5162.346	24.0	0.301	0.177
5162.346	24.0	0.301	0.177
5162.378	23.0	0.301	0.159
5162.378	23.0	0.301	0.159
5162.527	22.0	0.301	0.140
5162.527	22.0	0.301	0.140
5162.578	5.0	0.196	-0.472
5162.578	5.0	0.196	-0.472

Table 4—Continued

Wavelength (Å)	J''	χ (eV)	$\log gf$
5162.864	23.0	0.292	0.159
5162.864	23.0	0.292	0.159
5162.942	22.0	0.292	0.140
5162.942	22.0	0.292	0.140
5163.049	21.0	0.292	0.120
5163.049	21.0	0.292	0.120
5163.134	7.0	0.198	-0.337
5163.134	7.0	0.198	-0.337
5163.420	21.0	0.283	0.120
5163.420	22.0	0.283	0.140
5163.420	22.0	0.283	0.140
5163.420	21.0	0.283	0.120
5163.597	20.0	0.283	0.100
5163.597	8.0	0.201	-0.283
5163.597	20.0	0.283	0.100
5163.597	7.0	0.202	-0.337
5163.597	8.0	0.201	-0.283
5163.597	7.0	0.202	-0.337
5163.808	21.0	0.274	0.120
5163.808	21.0	0.274	0.120
5163.841	20.0	0.275	0.100

Table 4—Continued

Wavelength (Å)	J''	χ (eV)	$\log gf$
5163.841	20.0	0.275	0.100
5163.988	9.0	0.204	-0.234
5163.988	19.0	0.275	0.078
5163.988	9.0	0.204	-0.234
5163.988	19.0	0.275	0.078
5164.074	8.0	0.205	-0.283
5164.074	7.0	0.205	-0.337
5164.074	7.0	0.205	-0.337
5164.074	8.0	0.205	-0.283
5164.255	10.0	0.208	-0.191
5164.255	20.0	0.266	0.100
5164.255	19.0	0.267	0.078
5164.255	10.0	0.208	-0.191
5164.255	20.0	0.266	0.100
5164.255	19.0	0.267	0.078
5164.378	18.0	0.267	0.055
5164.378	18.0	0.267	0.055
5164.406	9.0	0.208	-0.234
5164.406	9.0	0.208	-0.234
5164.406	8.0	0.209	-0.283
5164.406	8.0	0.209	-0.283

Table 4—Continued

Wavelength (Å)	J''	χ (eV)	$\log gf$
5164.510	19.0	0.259	0.078
5164.510	19.0	0.259	0.078
5164.539	18.0	0.259	0.055
5164.539	11.0	0.212	-0.151
5164.539	11.0	0.212	-0.151
5164.539	18.0	0.259	0.055
5164.674	10.0	0.212	-0.191
5164.674	17.0	0.259	0.031
5164.674	17.0	0.259	0.031
5164.674	10.0	0.212	-0.191
5164.753	12.0	0.216	-0.115
5164.753	18.0	0.251	0.055
5164.753	17.0	0.252	0.031
5164.753	9.0	0.213	-0.234
5164.753	12.0	0.216	-0.115
5164.753	17.0	0.252	0.031
5164.753	18.0	0.251	0.055
5164.753	9.0	0.213	-0.234
5164.900	17.0	0.245	0.031
5164.900	13.0	0.221	-0.082
5164.900	10.0	0.217	-0.191

Table 4—Continued

Wavelength (Å)	J''	χ (eV)	$\log gf$
5164.900	17.0	0.245	0.031
5164.900	16.0	0.245	0.006
5164.900	16.0	0.252	0.006
5164.900	16.0	0.252	0.006
5164.900	11.0	0.217	-0.151
5164.900	16.0	0.245	0.006
5164.900	10.0	0.217	-0.191
5164.900	13.0	0.221	-0.082
5164.900	11.0	0.217	-0.151
5165.026	12.0	0.222	-0.115
5165.026	12.0	0.222	-0.115
5165.026	15.0	0.238	-0.022
5165.026	15.0	0.245	-0.022
5165.026	15.0	0.245	-0.022
5165.026	14.0	0.226	-0.051
5165.026	14.0	0.226	-0.051
5165.026	13.0	0.227	-0.082
5165.026	13.0	0.227	-0.082
5165.026	15.0	0.238	-0.022
5165.026	14.0	0.233	-0.051
5165.026	15.0	0.232	-0.022

Table 4—Continued

Wavelength (Å)	J''	χ (eV)	$\log gf$
5165.026	15.0	0.232	-0.022
5165.026	16.0	0.238	0.006
5165.026	11.0	0.222	-0.151
5165.026	14.0	0.233	-0.051
5165.026	16.0	0.238	0.006
5165.026	11.0	0.222	-0.151
5165.242	12.0	0.227	-0.115
5165.242	14.0	0.239	-0.051
5165.242	14.0	0.239	-0.051
5165.242	12.0	0.227	-0.115
5165.242	13.0	0.233	-0.082
5165.242	13.0	0.233	-0.082

Table 5. Molecular line list for the (0,0) C₂ swan band - ¹²C¹³C lines

Wavelength (Å)	J''	χ (eV)	$\log gf$
5132.755	47.0	0.640	0.465
5132.877	48.0	0.640	0.474
5131.091	47.0	0.640	0.465
5131.171	48.0	0.640	0.474
5132.735	46.0	0.640	0.455
5131.101	46.0	0.640	0.455
5131.816	19.0	0.259	0.078
5131.879	18.0	0.259	0.055
5131.965	17.0	0.259	0.031
5134.741	47.0	0.622	0.465
5134.627	46.0	0.622	0.455
5133.075	47.0	0.622	0.465
5132.992	46.0	0.622	0.455
5133.031	45.0	0.622	0.446
5134.626	45.0	0.622	0.446
5133.822	18.0	0.251	0.055
5133.880	17.0	0.252	0.031
5134.004	16.0	0.252	0.006
5135.128	46.0	0.603	0.455
5136.648	45.0	0.603	0.446
5136.765	46.0	0.603	0.455

Table 5—Continued

Wavelength (Å)	J''	χ (eV)	$\log gf$
5135.052	45.0	0.603	0.446
5135.079	44.0	0.604	0.436
5136.645	44.0	0.604	0.436
5135.703	17.0	0.245	0.031
5135.795	16.0	0.245	0.006
5135.902	15.0	0.245	-0.022
5136.841	44.0	0.586	0.436
5138.517	45.0	0.586	0.446
5136.920	45.0	0.586	0.446
5138.408	44.0	0.586	0.436
5136.877	43.0	0.586	0.427
5138.403	43.0	0.586	0.427
5137.581	16.0	0.238	0.006
5137.672	15.0	0.238	-0.022
5137.819	14.0	0.239	-0.051
5140.410	44.0	0.568	0.436
5140.298	43.0	0.568	0.427
5138.842	44.0	0.568	0.436
5138.771	43.0	0.568	0.427
5140.304	42.0	0.568	0.416
5138.808	42.0	0.568	0.416

Table 5—Continued

Wavelength (Å)	J''	χ (eV)	$\log gf$
5139.345	15.0	0.232	-0.022
5139.476	14.0	0.233	-0.051
5139.600	13.0	0.233	-0.082
5142.037	43.0	0.551	0.427
5141.933	42.0	0.551	0.416
5140.509	43.0	0.551	0.427
5140.435	42.0	0.551	0.416
5141.951	41.0	0.551	0.406
5140.494	41.0	0.551	0.406
5141.093	14.0	0.226	-0.051
5141.233	13.0	0.227	-0.082
5141.403	12.0	0.227	-0.115
5143.711	41.0	0.534	0.406
5142.253	41.0	0.534	0.406
5143.818	42.0	0.534	0.416
5142.319	42.0	0.534	0.416
5143.723	40.0	0.535	0.395
5142.296	40.0	0.535	0.395
5142.739	13.0	0.221	-0.082
5142.919	12.0	0.222	-0.115
5143.072	11.0	0.222	-0.151

Table 5—Continued

Wavelength (Å)	J''	χ (eV)	$\log gf$
5143.822	40.0	0.518	0.395
5145.350	41.0	0.518	0.406
5143.890	41.0	0.518	0.406
5145.250	40.0	0.518	0.395
5143.852	39.0	0.518	0.385
5145.240	39.0	0.518	0.385
5144.355	12.0	0.216	-0.115
5144.557	11.0	0.217	-0.151
5144.758	10.0	0.217	-0.191
5146.983	40.0	0.502	0.395
5145.493	39.0	0.502	0.385
5145.554	40.0	0.502	0.395
5146.882	39.0	0.502	0.385
5146.906	38.0	0.502	0.373
5145.548	38.0	0.502	0.373
5145.883	11.0	0.212	-0.151
5146.128	10.0	0.212	-0.191
5146.311	9.0	0.213	-0.234
5146.937	38.0	0.487	0.373
5147.000	39.0	0.487	0.385
5148.295	38.0	0.487	0.373

Table 5—Continued

Wavelength (Å)	J''	χ (eV)	$\log gf$
5148.390	39.0	0.487	0.385
5148.323	37.0	0.487	0.362
5147.005	37.0	0.487	0.362
5147.361	10.0	0.208	-0.191
5147.649	9.0	0.208	-0.234
5147.893	8.0	0.209	-0.283
5149.905	38.0	0.472	0.373
5148.546	38.0	0.472	0.373
5148.489	37.0	0.472	0.362
5149.809	37.0	0.472	0.362
5149.843	36.0	0.472	0.350
5148.556	36.0	0.472	0.350
5148.765	9.0	0.204	-0.234
5149.103	8.0	0.205	-0.283
5149.330	7.0	0.205	-0.337
5151.116	36.0	0.457	0.350
5149.828	36.0	0.457	0.350
5151.207	37.0	0.457	0.362
5149.887	37.0	0.457	0.362
5151.147	35.0	0.457	0.338
5149.898	35.0	0.457	0.338

Table 5—Continued

Wavelength (Å)	J''	χ (eV)	$\log gf$
5150.108	8.0	0.201	-0.283
5150.510	7.0	0.202	-0.337
5151.246	35.0	0.443	0.338
5151.299	36.0	0.442	0.350
5152.496	35.0	0.443	0.338
5152.587	36.0	0.442	0.350
5151.390	7.0	0.198	-0.337
5151.302	34.0	0.443	0.326
5152.519	34.0	0.443	0.326
5153.770	35.0	0.429	0.338
5152.520	35.0	0.429	0.338
5152.501	34.0	0.429	0.326
5153.718	34.0	0.429	0.326
5153.700	33.0	0.429	0.313
5152.521	33.0	0.429	0.313
5153.135	5.0	0.196	-0.472
5154.940	33.0	0.415	0.313
5153.760	33.0	0.415	0.313
5155.026	34.0	0.415	0.326
5153.808	34.0	0.415	0.326
5153.831	32.0	0.415	0.300

Table 5—Continued

Wavelength (Å)	J''	χ (eV)	$\log gf$
5154.978	32.0	0.415	0.300
5154.878	32.0	0.402	0.300
5154.926	33.0	0.402	0.313
5156.105	33.0	0.402	0.313
5156.024	32.0	0.402	0.300
5156.058	31.0	0.402	0.286
5154.950	31.0	0.402	0.286
5156.057	32.0	0.389	0.300
5157.204	32.0	0.389	0.300
5156.022	31.0	0.389	0.286
5157.131	31.0	0.389	0.286
5157.180	30.0	0.389	0.272
5156.104	30.0	0.389	0.272
5158.145	31.0	0.377	0.286
5157.035	31.0	0.377	0.286
5157.042	30.0	0.377	0.272
5158.118	30.0	0.377	0.272
5158.141	29.0	0.377	0.258
5157.103	29.0	0.377	0.258
5158.060	30.0	0.365	0.272
5159.137	30.0	0.365	0.272

Table 5—Continued

Wavelength (Å)	J''	χ (eV)	$\log gf$
5158.060	29.0	0.365	0.258
5159.099	29.0	0.365	0.258
5159.142	28.0	0.365	0.243
5158.138	28.0	0.365	0.243
5158.908	29.0	0.353	0.258
5159.946	29.0	0.353	0.258
5158.942	28.0	0.353	0.243
5159.947	28.0	0.353	0.243
5159.968	27.0	0.353	0.227
5159.001	27.0	0.353	0.227
5160.838	28.0	0.342	0.243
5159.833	28.0	0.342	0.243
5160.784	27.0	0.342	0.227
5159.817	27.0	0.342	0.227
5159.914	26.0	0.342	0.211
5160.848	26.0	0.342	0.211
5160.560	27.0	0.331	0.227
5161.527	27.0	0.331	0.227
5160.597	26.0	0.331	0.211
5161.531	26.0	0.331	0.211
5160.671	25.0	0.331	0.195

Table 5—Continued

Wavelength (Å)	J''	χ (eV)	$\log gf$
5161.567	25.0	0.331	0.195
5162.285	26.0	0.321	0.211
5161.351	26.0	0.321	0.211
5161.340	25.0	0.321	0.195
5162.236	25.0	0.321	0.195
5161.446	24.0	0.321	0.177
5162.309	24.0	0.321	0.177
5162.863	25.0	0.311	0.195
5161.966	25.0	0.311	0.195
5162.862	24.0	0.311	0.177
5162.000	24.0	0.311	0.177
5162.089	23.0	0.311	0.159
5162.914	23.0	0.311	0.159
5163.467	24.0	0.301	0.177
5162.605	24.0	0.301	0.177
5163.438	23.0	0.301	0.159
5162.613	23.0	0.301	0.159
5162.740	22.0	0.301	0.140
5163.530	22.0	0.301	0.140
5162.805	5.0	0.196	-0.472
5162.985	5.0	0.196	-0.472

Table 5—Continued

Wavelength (Å)	J''	χ (eV)	$\log gf$
5163.099	23.0	0.292	0.159
5163.924	23.0	0.292	0.159
5163.945	22.0	0.292	0.140
5163.155	22.0	0.292	0.140
5163.243	21.0	0.292	0.120
5163.997	21.0	0.292	0.120
5163.322	7.0	0.198	-0.337
5163.573	7.0	0.198	-0.337
5163.614	21.0	0.283	0.120
5163.633	22.0	0.283	0.140
5164.424	22.0	0.283	0.140
5164.368	21.0	0.283	0.120
5164.493	20.0	0.283	0.100
5164.056	8.0	0.201	-0.283
5163.774	20.0	0.283	0.100
5164.036	7.0	0.202	-0.337
5163.769	8.0	0.201	-0.283
5163.785	7.0	0.202	-0.337
5164.002	21.0	0.274	0.120
5164.756	21.0	0.274	0.120
5164.018	20.0	0.275	0.100

Table 5—Continued

Wavelength (Å)	J''	χ (eV)	$\log gf$
5164.737	20.0	0.275	0.100
5164.470	9.0	0.204	-0.234
5164.833	19.0	0.275	0.078
5164.147	9.0	0.204	-0.234
5164.151	19.0	0.275	0.078
5164.534	8.0	0.205	-0.283
5164.513	7.0	0.205	-0.337
5164.262	7.0	0.205	-0.337
5164.246	8.0	0.205	-0.283
5164.762	10.0	0.208	-0.191
5165.151	20.0	0.266	0.100
5165.100	19.0	0.267	0.078
5164.403	10.0	0.208	-0.191
5164.432	20.0	0.266	0.100
5164.418	19.0	0.267	0.078
5165.176	18.0	0.267	0.055
5164.529	18.0	0.267	0.055
5164.888	9.0	0.208	-0.234
5164.565	9.0	0.208	-0.234
5164.866	8.0	0.209	-0.283
5164.578	8.0	0.209	-0.283

Table 5—Continued

Wavelength (Å)	J''	χ (eV)	$\log gf$
5164.673	19.0	0.259	0.078
5165.355	19.0	0.259	0.078
5165.337	18.0	0.259	0.055
5165.074	11.0	0.212	-0.151
5164.679	11.0	0.212	-0.151
5164.690	18.0	0.259	0.055
5165.181	10.0	0.212	-0.191
5165.427	17.0	0.259	0.031
5164.816	17.0	0.259	0.031
5164.822	10.0	0.212	-0.191
5165.318	12.0	0.216	-0.115
5165.551	18.0	0.251	0.055
5164.895	17.0	0.252	0.031
5164.912	9.0	0.213	-0.234
5164.887	12.0	0.216	-0.115
5165.506	17.0	0.252	0.031
5164.904	18.0	0.251	0.055
5165.235	9.0	0.213	-0.234
5165.653	17.0	0.245	0.031
5165.497	13.0	0.221	-0.082
5165.407	10.0	0.217	-0.191

Table 5—Continued

Wavelength (Å)	J''	χ (eV)	$\log gf$
5165.042	17.0	0.245	0.031
5165.611	16.0	0.245	0.006
5165.611	16.0	0.252	0.006
5165.035	16.0	0.252	0.006
5165.040	11.0	0.217	-0.151
5165.035	16.0	0.245	0.006
5165.048	10.0	0.217	-0.191
5165.031	13.0	0.221	-0.082
5165.435	11.0	0.217	-0.151
5165.591	12.0	0.222	-0.115
5165.160	12.0	0.222	-0.115
5165.696	15.0	0.238	-0.022
5165.157	15.0	0.245	-0.022
5165.696	15.0	0.245	-0.022
5165.659	14.0	0.226	-0.051
5165.155	14.0	0.226	-0.051
5165.623	13.0	0.227	-0.082
5165.157	13.0	0.227	-0.082
5165.157	15.0	0.238	-0.022
5165.155	14.0	0.233	-0.051
5165.157	15.0	0.232	-0.022

Table 5—Continued

Wavelength (Å)	J''	χ (eV)	$\log gf$
5165.696	15.0	0.232	-0.022
5165.161	16.0	0.238	0.006
5165.166	11.0	0.222	-0.151
5165.659	14.0	0.233	-0.051
5165.737	16.0	0.238	0.006
5165.561	11.0	0.222	-0.151
5165.807	12.0	0.227	-0.115
5165.875	14.0	0.239	-0.051
5165.371	14.0	0.239	-0.051
5165.376	12.0	0.227	-0.115
5165.840	13.0	0.233	-0.082
5165.373	13.0	0.233	-0.082

Table 6. Molecular line list for the (0, 1) C₂ swan band - ¹²C¹²C lines

Wavelength (Å)	J''	χ (eV)	$\log gf$
5587.533	21.0	0.474	-0.360
5587.684	20.0	0.474	-0.381
5587.876	19.0	0.475	-0.403
5588.125	45.0	0.800	-0.035
5588.125	45.0	0.800	-0.035
5588.125	46.0	0.800	-0.025
5588.125	46.0	0.800	-0.025
5588.263	44.0	0.800	-0.044
5588.263	44.0	0.800	-0.044
5590.368	20.0	0.466	-0.381
5590.512	19.0	0.466	-0.403
5590.746	18.0	0.467	-0.425
5590.831	44.0	0.782	-0.044
5590.831	45.0	0.782	-0.035
5590.831	45.0	0.782	-0.035
5590.831	44.0	0.782	-0.044
5590.953	43.0	0.782	-0.054
5590.953	43.0	0.782	-0.054
5593.040	19.0	0.459	-0.403
5593.220	18.0	0.459	-0.425
5593.423	17.0	0.459	-0.450

Table 6—Continued

Wavelength (Å)	J''	χ (eV)	$\log gf$
5593.640	43.0	0.765	-0.054
5593.640	43.0	0.765	-0.054
5593.640	44.0	0.765	-0.044
5593.640	44.0	0.765	-0.044
5593.771	42.0	0.765	-0.064
5593.771	42.0	0.765	-0.064
5595.700	18.0	0.451	-0.425
5595.872	17.0	0.452	-0.450
5596.122	16.0	0.452	-0.475
5596.160	43.0	0.748	-0.054
5596.160	42.0	0.748	-0.064
5596.160	42.0	0.748	-0.064
5596.160	43.0	0.748	-0.054
5596.321	41.0	0.748	-0.074
5596.321	41.0	0.748	-0.074
5598.212	17.0	0.445	-0.450
5598.420	16.0	0.445	-0.475
5598.640	15.0	0.445	-0.502
5598.817	42.0	0.731	-0.064
5598.817	41.0	0.732	-0.074
5598.817	41.0	0.732	-0.074

Table 6—Continued

Wavelength (Å)	J''	χ (eV)	$\log gf$
5598.817	42.0	0.731	-0.064
5598.958	40.0	0.732	-0.085
5598.958	40.0	0.732	-0.085
5600.697	16.0	0.438	-0.475
5600.909	15.0	0.439	-0.502
5601.175	14.0	0.439	-0.531
5601.203	41.0	0.715	-0.074
5601.203	41.0	0.715	-0.074
5601.203	40.0	0.716	-0.085
5601.203	40.0	0.716	-0.085
5601.348	39.0	0.716	-0.096
5601.348	39.0	0.716	-0.096
5603.043	15.0	0.432	-0.502
5603.293	14.0	0.433	-0.531
5603.534	13.0	0.433	-0.562
5603.663	39.0	0.700	-0.096
5603.663	40.0	0.700	-0.085
5603.663	40.0	0.700	-0.085
5603.663	39.0	0.700	-0.096
5603.803	38.0	0.700	-0.107
5603.803	38.0	0.700	-0.107

Table 6—Continued

Wavelength (Å)	J''	χ (eV)	$\log gf$
5605.349	14.0	0.427	-0.531
5605.610	13.0	0.427	-0.562
5605.900	39.0	0.684	-0.096
5605.900	38.0	0.684	-0.107
5605.900	39.0	0.684	-0.096
5605.900	38.0	0.684	-0.107
5605.900	12.0	0.427	-0.596
5606.037	37.0	0.685	-0.119
5606.037	37.0	0.685	-0.119
5606.037	37.0	0.685	-0.119
5607.834	12.0	0.422	-0.596
5608.108	11.0	0.422	-0.632
5608.173	37.0	0.669	-0.119
5608.173	38.0	0.669	-0.107
5608.173	37.0	0.669	-0.119
5608.173	38.0	0.669	-0.107
5608.317	36.0	0.670	-0.130
5608.317	36.0	0.670	-0.130
5609.657	12.0	0.417	-0.596
5609.988	11.0	0.417	-0.632
5610.239	37.0	0.655	-0.119

Table 6—Continued

Wavelength (Å)	J''	χ (eV)	$\log gf$
5610.239	37.0	0.655	-0.119
5610.300	36.0	0.655	-0.130
5610.300	36.0	0.655	-0.130
5610.365	35.0	0.655	-0.142
5610.365	35.0	0.655	-0.142
5611.667	11.0	0.412	-0.632
5612.044	10.0	0.413	-0.671
5612.339	36.0	0.640	-0.130
5612.339	35.0	0.641	-0.142
5612.339	35.0	0.641	-0.142
5612.339	9.0	0.413	-0.715
5612.339	36.0	0.640	-0.130
5612.489	34.0	0.641	-0.155
5612.489	34.0	0.641	-0.155
5613.609	10.0	0.408	-0.671
5614.031	9.0	0.409	-0.715
5614.228	35.0	0.627	-0.142
5614.228	35.0	0.627	-0.142
5614.252	34.0	0.627	-0.155
5614.252	34.0	0.627	-0.155
5614.391	33.0	0.627	-0.167

Table 6—Continued

Wavelength (Å)	J''	χ (eV)	$\log gf$
5614.391	8.0	0.409	-0.763
5614.391	33.0	0.627	-0.167
5615.436	9.0	0.405	-0.715
5615.917	8.0	0.405	-0.763
5616.162	34.0	0.613	-0.155
5616.162	34.0	0.613	-0.155
5616.162	33.0	0.613	-0.167
5616.162	33.0	0.613	-0.167
5616.285	7.0	0.406	-0.818
5616.305	32.0	0.614	-0.181
5616.305	32.0	0.614	-0.181
5617.190	8.0	0.401	-0.763
5617.745	7.0	0.402	-0.818
5617.888	33.0	0.600	-0.167
5617.888	33.0	0.600	-0.167
5617.912	32.0	0.600	-0.181
5617.912	32.0	0.600	-0.181
5618.053	31.0	0.601	-0.194
5618.053	31.0	0.601	-0.194
5619.644	32.0	0.588	-0.181
5619.644	31.0	0.588	-0.194

Table 6—Continued

Wavelength (Å)	J''	χ (eV)	$\log gf$
5619.644	32.0	0.588	-0.181
5619.644	31.0	0.588	-0.194
5619.811	30.0	0.588	-0.208
5619.811	30.0	0.588	-0.208
5621.158	5.0	0.397	-0.952
5621.177	31.0	0.575	-0.194
5621.177	31.0	0.575	-0.194
5621.236	30.0	0.576	-0.208
5621.236	30.0	0.576	-0.208
5621.369	29.0	0.576	-0.223
5621.369	29.0	0.576	-0.223
5622.780	30.0	0.563	-0.208
5622.780	29.0	0.564	-0.223
5622.780	30.0	0.563	-0.208
5622.780	29.0	0.564	-0.223
5622.945	28.0	0.564	-0.238
5622.945	28.0	0.564	-0.238
5624.162	29.0	0.552	-0.223
5624.162	29.0	0.552	-0.223
5624.204	28.0	0.552	-0.238
5624.204	28.0	0.552	-0.238

Table 6—Continued

Wavelength (Å)	J''	χ (eV)	$\log gf$
5624.345	27.0	0.552	-0.253
5624.345	27.0	0.552	-0.253
5625.565	27.0	0.541	-0.253
5625.565	28.0	0.541	-0.238
5625.565	27.0	0.541	-0.253
5625.565	28.0	0.541	-0.238
5625.735	26.0	0.541	-0.269
5625.735	26.0	0.541	-0.269
5626.765	27.0	0.530	-0.253
5626.765	27.0	0.530	-0.253
5626.825	26.0	0.530	-0.269
5626.825	26.0	0.530	-0.269
5626.962	25.0	0.530	-0.286
5626.962	25.0	0.530	-0.286
5628.002	26.0	0.520	-0.269
5628.002	26.0	0.520	-0.269
5628.002	25.0	0.520	-0.286
5628.002	25.0	0.520	-0.286
5628.192	24.0	0.520	-0.303
5628.192	24.0	0.520	-0.303
5629.038	25.0	0.510	-0.286

Table 6—Continued

Wavelength (Å)	J''	χ (eV)	$\log gf$
5629.038	25.0	0.510	-0.286
5629.107	24.0	0.510	-0.303
5629.107	24.0	0.510	-0.303
5629.243	23.0	0.510	-0.321
5629.243	23.0	0.510	-0.321
5630.072	24.0	0.500	-0.303
5630.072	24.0	0.500	-0.303
5630.118	23.0	0.501	-0.321
5630.118	23.0	0.501	-0.321
5630.280	22.0	0.501	-0.340
5630.280	22.0	0.501	-0.340
5630.956	23.0	0.491	-0.321
5630.956	23.0	0.491	-0.321
5631.025	22.0	0.491	-0.340
5631.025	22.0	0.491	-0.340
5631.166	21.0	0.492	-0.360
5631.166	21.0	0.492	-0.360
5631.795	22.0	0.482	-0.340
5631.795	22.0	0.482	-0.340
5631.858	21.0	0.483	-0.360
5631.858	21.0	0.483	-0.360

Table 6—Continued

Wavelength (Å)	J''	χ (eV)	$\log gf$
5632.028	20.0	0.483	-0.381
5632.028	20.0	0.483	-0.381
5632.514	21.0	0.474	-0.360
5632.514	21.0	0.474	-0.360
5632.598	20.0	0.474	-0.381
5632.598	20.0	0.474	-0.381
5632.742	19.0	0.475	-0.403
5632.742	19.0	0.475	-0.403
5633.090	5.0	0.397	-0.952
5633.090	5.0	0.397	-0.952
5633.180	20.0	0.466	-0.381
5633.180	20.0	0.466	-0.381
5633.236	19.0	0.466	-0.403
5633.236	19.0	0.466	-0.403
5633.423	18.0	0.467	-0.425
5633.423	18.0	0.467	-0.425
5633.732	19.0	0.459	-0.403
5633.732	19.0	0.459	-0.403
5633.814	18.0	0.459	-0.425
5633.814	18.0	0.459	-0.425
5633.965	17.0	0.459	-0.450

Table 6—Continued

Wavelength (Å)	J''	χ (eV)	$\log gf$
5633.965	17.0	0.459	-0.450
5634.114	8.0	0.401	-0.763
5634.114	8.0	0.401	-0.763
5634.217	18.0	0.451	-0.425
5634.217	18.0	0.451	-0.425
5634.217	7.0	0.402	-0.818
5634.217	7.0	0.402	-0.818
5634.305	17.0	0.452	-0.450
5634.305	17.0	0.452	-0.450
5634.484	9.0	0.405	-0.715
5634.484	9.0	0.405	-0.715
5634.484	16.0	0.452	-0.475
5634.484	16.0	0.452	-0.475
5634.598	8.0	0.405	-0.763
5634.598	17.0	0.445	-0.450
5634.598	8.0	0.405	-0.763
5634.598	17.0	0.445	-0.450
5634.705	7.0	0.406	-0.818
5634.705	7.0	0.406	-0.818
5634.705	16.0	0.445	-0.475
5634.705	16.0	0.445	-0.475

Table 6—Continued

Wavelength (Å)	J''	χ (eV)	$\log gf$
5634.835	15.0	0.445	-0.502
5634.835	10.0	0.408	-0.671
5634.835	10.0	0.408	-0.671
5634.835	15.0	0.445	-0.502
5634.913	9.0	0.409	-0.715
5634.913	16.0	0.438	-0.475
5634.913	16.0	0.438	-0.475
5634.913	9.0	0.409	-0.715
5634.964	15.0	0.439	-0.502
5634.964	15.0	0.439	-0.502
5635.079	15.0	0.432	-0.502
5635.079	11.0	0.412	-0.632
5635.079	15.0	0.432	-0.502
5635.079	8.0	0.409	-0.763
5635.079	11.0	0.412	-0.632
5635.079	8.0	0.409	-0.763
5635.195	10.0	0.413	-0.671
5635.195	10.0	0.413	-0.671
5635.195	14.0	0.433	-0.531
5635.195	14.0	0.439	-0.531
5635.195	14.0	0.439	-0.531

Table 6—Continued

Wavelength (Å)	J''	χ (eV)	$\log gf$
5635.195	14.0	0.433	-0.531
5635.202	13.0	0.421	-0.562
5635.202	13.0	0.421	-0.562
5635.202	14.0	0.427	-0.531
5635.202	12.0	0.417	-0.596
5635.202	14.0	0.427	-0.531
5635.202	12.0	0.417	-0.596
5635.324	9.0	0.413	-0.715
5635.324	9.0	0.413	-0.715
5635.324	11.0	0.417	-0.632
5635.324	11.0	0.417	-0.632
5635.333	12.0	0.422	-0.596
5635.333	13.0	0.433	-0.562
5635.333	12.0	0.422	-0.596
5635.333	13.0	0.433	-0.562
5635.333	13.0	0.427	-0.562
5635.333	13.0	0.427	-0.562
5635.490	10.0	0.418	-0.671
5635.490	10.0	0.418	-0.671
5635.499	12.0	0.427	-0.596
5635.499	11.0	0.422	-0.632

Table 6—Continued

Wavelength (Å)	J''	χ (eV)	$\log gf$
5635.499	11.0	0.422	-0.632
5635.499	12.0	0.427	-0.596

Table 7. Molecular line list for the (0, 1) C₂ swan band - ¹²C¹³C lines

Wavelength (Å)	J''	χ (eV)	$\log gf$
5579.970	21.0	0.474	-0.360
5580.008	20.0	0.474	-0.381
5580.092	19.0	0.475	-0.403
5582.309	45.0	0.800	-0.035
5580.424	45.0	0.800	-0.035
5582.465	46.0	0.800	-0.025
5580.532	46.0	0.800	-0.025
5582.300	44.0	0.800	-0.044
5580.451	44.0	0.800	-0.044
5582.684	20.0	0.466	-0.381
5582.720	19.0	0.466	-0.403
5582.848	18.0	0.467	-0.425
5584.863	44.0	0.782	-0.044
5583.123	45.0	0.782	-0.035
5585.009	45.0	0.782	-0.035
5583.012	44.0	0.782	-0.044
5583.032	43.0	0.782	-0.054
5584.835	43.0	0.782	-0.054
5585.241	19.0	0.459	-0.403
5585.315	18.0	0.459	-0.425
5585.416	17.0	0.459	-0.450

Table 7—Continued

Wavelength (Å)	J''	χ (eV)	$\log gf$
5587.516	43.0	0.765	-0.054
5585.711	43.0	0.765	-0.054
5585.813	44.0	0.765	-0.044
5587.666	44.0	0.765	-0.044
5587.506	42.0	0.765	-0.064
5585.738	42.0	0.765	-0.064
5587.788	18.0	0.451	-0.425
5587.858	17.0	0.452	-0.450
5588.008	16.0	0.452	-0.475
5588.224	43.0	0.748	-0.054
5588.120	42.0	0.748	-0.064
5589.890	42.0	0.748	-0.064
5590.030	43.0	0.748	-0.054
5589.908	41.0	0.748	-0.074
5588.185	41.0	0.748	-0.074
5590.191	17.0	0.445	-0.450
5590.299	16.0	0.445	-0.475
5590.424	15.0	0.445	-0.502
5592.541	42.0	0.731	-0.064
5590.674	41.0	0.732	-0.074
5592.398	41.0	0.732	-0.074

Table 7—Continued

Wavelength (Å)	J''	χ (eV)	$\log gf$
5590.769	42.0	0.731	-0.064
5590.717	40.0	0.732	-0.085
5592.404	40.0	0.732	-0.085
5592.570	16.0	0.438	-0.475
5592.686	15.0	0.439	-0.502
5592.858	14.0	0.439	-0.531
5594.778	41.0	0.715	-0.074
5593.053	41.0	0.715	-0.074
5592.956	40.0	0.716	-0.085
5594.644	40.0	0.716	-0.085
5594.653	39.0	0.716	-0.096
5593.011	39.0	0.716	-0.096
5594.814	15.0	0.432	-0.502
5594.970	14.0	0.433	-0.531
5595.122	13.0	0.433	-0.562
5595.319	39.0	0.700	-0.096
5595.409	40.0	0.700	-0.085
5597.098	40.0	0.700	-0.085
5596.962	39.0	0.700	-0.096
5596.974	38.0	0.700	-0.107
5595.369	38.0	0.700	-0.107

Table 7—Continued

Wavelength (Å)	J''	χ (eV)	$\log gf$
5597.020	14.0	0.427	-0.531
5597.192	13.0	0.427	-0.562
5599.194	39.0	0.684	-0.096
5599.066	38.0	0.684	-0.107
5597.550	39.0	0.684	-0.096
5597.459	38.0	0.684	-0.107
5597.395	12.0	0.427	-0.596
5599.073	37.0	0.685	-0.119
5599.073	37.0	0.685	-0.119
5597.513	37.0	0.685	-0.119
5599.323	12.0	0.422	-0.596
5599.514	11.0	0.422	-0.632
5599.643	37.0	0.669	-0.119
5599.725	38.0	0.669	-0.107
5601.203	37.0	0.669	-0.119
5601.333	38.0	0.669	-0.107
5599.703	36.0	0.670	-0.130
5601.225	36.0	0.670	-0.130
5601.140	12.0	0.417	-0.596
5601.388	11.0	0.417	-0.632
5601.702	37.0	0.655	-0.119

Table 7—Continued

Wavelength (Å)	J''	χ (eV)	$\log gf$
5603.264	37.0	0.655	-0.119
5603.203	36.0	0.655	-0.130
5601.679	36.0	0.655	-0.130
5601.668	35.0	0.655	-0.142
5603.145	35.0	0.655	-0.142
5603.062	11.0	0.412	-0.632
5603.358	10.0	0.413	-0.671
5605.237	36.0	0.640	-0.130
5603.636	35.0	0.641	-0.142
5605.114	35.0	0.641	-0.142
5603.577	9.0	0.413	-0.715
5603.712	36.0	0.640	-0.130
5603.708	34.0	0.641	-0.155
5605.149	34.0	0.641	-0.155
5604.919	10.0	0.408	-0.671
5605.264	9.0	0.409	-0.715
5606.999	35.0	0.627	-0.142
5605.519	35.0	0.627	-0.142
5606.907	34.0	0.627	-0.155
5605.466	34.0	0.627	-0.155
5605.534	33.0	0.627	-0.167

Table 7—Continued

Wavelength (Å)	J''	χ (eV)	$\log gf$
5605.550	8.0	0.409	-0.763
5606.930	33.0	0.627	-0.167
5606.664	9.0	0.405	-0.715
5607.071	8.0	0.405	-0.763
5608.812	34.0	0.613	-0.155
5607.370	34.0	0.613	-0.155
5608.696	33.0	0.613	-0.167
5607.300	33.0	0.613	-0.167
5607.369	7.0	0.406	-0.818
5608.729	32.0	0.614	-0.181
5607.372	32.0	0.614	-0.181
5608.340	8.0	0.401	-0.763
5608.824	7.0	0.402	-0.818
5610.417	33.0	0.600	-0.167
5609.020	33.0	0.600	-0.167
5610.332	32.0	0.600	-0.181
5608.974	32.0	0.600	-0.181
5610.364	31.0	0.601	-0.194
5609.051	31.0	0.601	-0.194
5612.059	32.0	0.588	-0.181
5610.637	31.0	0.588	-0.194

Table 7—Continued

Wavelength (Å)	J''	χ (eV)	$\log gf$
5610.701	32.0	0.588	-0.181
5611.950	31.0	0.588	-0.194
5610.740	30.0	0.588	-0.208
5612.014	30.0	0.588	-0.208
5612.098	5.0	0.397	-0.952
5613.479	31.0	0.575	-0.194
5612.165	31.0	0.575	-0.194
5612.161	30.0	0.576	-0.208
5613.435	30.0	0.576	-0.208
5612.236	29.0	0.576	-0.223
5613.465	29.0	0.576	-0.223
5613.700	30.0	0.563	-0.208
5614.872	29.0	0.564	-0.223
5614.975	30.0	0.563	-0.208
5613.643	29.0	0.564	-0.223
5613.751	28.0	0.564	-0.238
5614.941	28.0	0.564	-0.238
5615.020	29.0	0.552	-0.223
5616.251	29.0	0.552	-0.223
5616.196	28.0	0.552	-0.238
5615.006	28.0	0.552	-0.238

Table 7—Continued

Wavelength (Å)	J''	χ (eV)	$\log gf$
5615.096	27.0	0.552	-0.253
5616.241	27.0	0.552	-0.253
5616.312	27.0	0.541	-0.253
5617.553	28.0	0.541	-0.238
5617.458	27.0	0.541	-0.253
5616.362	28.0	0.541	-0.238
5616.431	26.0	0.541	-0.269
5617.537	26.0	0.541	-0.269
5617.508	27.0	0.530	-0.253
5618.654	27.0	0.530	-0.253
5618.624	26.0	0.530	-0.269
5617.518	26.0	0.530	-0.269
5617.610	25.0	0.530	-0.286
5618.672	25.0	0.530	-0.286
5619.798	26.0	0.520	-0.269
5618.691	26.0	0.520	-0.269
5619.709	25.0	0.520	-0.286
5618.647	25.0	0.520	-0.286
5618.794	24.0	0.520	-0.303
5619.815	24.0	0.520	-0.303
5620.742	25.0	0.510	-0.286

Table 7—Continued

Wavelength (Å)	J''	χ (eV)	$\log gf$
5619.679	25.0	0.510	-0.286
5620.727	24.0	0.510	-0.303
5619.706	24.0	0.510	-0.303
5620.781	23.0	0.510	-0.321
5619.804	23.0	0.510	-0.321
5621.690	24.0	0.500	-0.303
5620.667	24.0	0.500	-0.303
5621.654	23.0	0.501	-0.321
5620.676	23.0	0.501	-0.321
5621.738	22.0	0.501	-0.340
5620.801	22.0	0.501	-0.340
5622.489	23.0	0.491	-0.321
5621.511	23.0	0.491	-0.321
5621.544	22.0	0.491	-0.340
5622.481	22.0	0.491	-0.340
5621.653	21.0	0.492	-0.360
5622.547	21.0	0.492	-0.360
5622.311	22.0	0.482	-0.340
5623.249	22.0	0.482	-0.340
5623.236	21.0	0.483	-0.360
5622.343	21.0	0.483	-0.360

Table 7—Continued

Wavelength (Å)	J''	χ (eV)	$\log gf$
5623.336	20.0	0.483	-0.381
5622.483	20.0	0.483	-0.381
5622.997	21.0	0.474	-0.360
5623.890	21.0	0.474	-0.360
5623.052	20.0	0.474	-0.381
5623.904	20.0	0.474	-0.381
5623.979	19.0	0.475	-0.403
5623.171	19.0	0.475	-0.403
5623.523	5.0	0.397	-0.952
5623.736	5.0	0.397	-0.952
5624.484	20.0	0.466	-0.381
5623.632	20.0	0.466	-0.381
5623.663	19.0	0.466	-0.403
5624.472	19.0	0.466	-0.403
5623.827	18.0	0.467	-0.425
5624.595	18.0	0.467	-0.425
5624.157	19.0	0.459	-0.403
5624.966	19.0	0.459	-0.403
5624.217	18.0	0.459	-0.425
5624.984	18.0	0.459	-0.425
5625.074	17.0	0.459	-0.450

Table 7—Continued

Wavelength (Å)	J''	χ (eV)	$\log gf$
5624.350	17.0	0.459	-0.450
5624.827	8.0	0.401	-0.763
5624.486	8.0	0.401	-0.763
5624.619	18.0	0.451	-0.425
5625.386	18.0	0.451	-0.425
5624.903	7.0	0.402	-0.818
5624.605	7.0	0.402	-0.818
5624.689	17.0	0.452	-0.450
5625.413	17.0	0.452	-0.450
5625.226	9.0	0.405	-0.715
5624.843	9.0	0.405	-0.715
5624.852	16.0	0.452	-0.475
5625.534	16.0	0.452	-0.475
5624.969	8.0	0.405	-0.763
5624.981	17.0	0.445	-0.450
5625.310	8.0	0.405	-0.763
5625.705	17.0	0.445	-0.450
5625.091	7.0	0.406	-0.818
5625.389	7.0	0.406	-0.818
5625.754	16.0	0.445	-0.475
5625.072	16.0	0.445	-0.475

Table 7—Continued

Wavelength (Å)	J''	χ (eV)	$\log gf$
5625.829	15.0	0.445	-0.502
5625.610	10.0	0.408	-0.671
5625.184	10.0	0.408	-0.671
5625.190	15.0	0.445	-0.502
5625.270	9.0	0.409	-0.715
5625.962	16.0	0.438	-0.475
5625.279	16.0	0.438	-0.475
5625.654	9.0	0.409	-0.715
5625.958	15.0	0.439	-0.502
5625.319	15.0	0.439	-0.502
5626.073	15.0	0.432	-0.502
5625.422	11.0	0.412	-0.632
5625.434	15.0	0.432	-0.502
5625.789	8.0	0.409	-0.763
5625.890	11.0	0.412	-0.632
5625.448	8.0	0.409	-0.763
5625.969	10.0	0.413	-0.671
5625.543	10.0	0.413	-0.671
5625.541	14.0	0.433	-0.531
5626.138	14.0	0.439	-0.531
5625.541	14.0	0.439	-0.531

Table 7—Continued

Wavelength (Å)	J''	χ (eV)	$\log gf$
5626.138	14.0	0.433	-0.531
5626.097	13.0	0.421	-0.562
5625.543	13.0	0.421	-0.562
5625.548	14.0	0.427	-0.531
5625.542	12.0	0.417	-0.596
5626.145	14.0	0.427	-0.531
5626.054	12.0	0.417	-0.596
5625.680	9.0	0.413	-0.715
5626.064	9.0	0.413	-0.715
5625.666	11.0	0.417	-0.632
5626.135	11.0	0.417	-0.632
5625.672	12.0	0.422	-0.596
5625.674	13.0	0.433	-0.562
5626.184	12.0	0.422	-0.596
5626.228	13.0	0.433	-0.562
5625.674	13.0	0.427	-0.562
5626.228	13.0	0.427	-0.562
5625.837	10.0	0.418	-0.671
5626.263	10.0	0.418	-0.671
5625.838	12.0	0.427	-0.596
5625.840	11.0	0.422	-0.632

Table 7—Continued

Wavelength (Å)	J''	χ (eV)	$\log gf$
5626.309	11.0	0.422	-0.632
5626.350	12.0	0.427	-0.596

Table 8. The atomic line list used in the syntheses of the (1, 0) C₂ swan band region with the individual estimates of the log gf -values from the γ Cyg, Sun, and Arcturus spectra and the adopted log gf -values.

Line	χ (eV)	$\log gf_{\gamma \text{Cyg}}^{\text{a}}$	$\log gf_{\text{Sun}}^{\text{b}}$	$\log gf_{\text{Arcturus}}^{\text{c}}$	$\log gf_{\text{Source}}$	Source	$\log gf_{\text{adopted}}$
Fe I λ 4729.018	4.07	-1.72	-1.60	-1.70	-1.61	NIST	-1.72
Ni I λ 4729.280	4.10	-2.00	-1.20	...	-1.20	NIST	-2.00
Fe I λ 4729.676	3.40	-2.36	-2.32	-2.50	-2.42	NIST	-2.36
Mg I λ 4730.028	4.34	-2.49	-2.42	-2.49	-2.34	NIST	-2.49
Cr I λ 4730.710	3.08	-0.48	-0.38	-0.38	-0.19	NIST	-0.48
Ti I λ 4731.165	2.17	...	-0.51	-0.51	-0.41	Kurucz	-0.51
Ni I λ 4731.798	3.83	...	-0.93	-1.10	-0.85	NIST	-0.93
Ni I λ 4732.457	4.10	-0.59	-0.55	...	-0.55	NIST	-0.59
Ti I λ 4733.421	2.16	...	-0.70	-0.65	-0.40	Kurucz	-0.70
Fe I λ 4733.591	1.48	-3.17	-3.03	-3.03	-2.98	NIST	-3.17
Fe I λ 4734.098	4.29	-1.60	-1.57	-1.43	-1.56	NIST	-1.60
Cr I λ 4734.260	7.94	-2.36	NIST	...
Ti I λ 4734.670	2.24	...	-0.87	-0.87	-0.86	Kurucz	-0.87
Cr I λ 4734.917	7.94	-4.29	NIST	...
Cr I λ 4735.163	7.94	-3.11	NIST	...
Fe I λ 4735.843	4.07	-1.12	-1.22	-1.32	-1.22	Kurucz	-1.12
Fe I λ 4736.773	3.21	-0.88	-0.75	-0.90	-0.75	NIST	-0.88
Cr I λ 4737.355	3.09	0.00	-0.30	-0.30	-0.09	NIST	0.00
Fe I λ 4737.635	3.26	-2.55	-2.50	-2.45	-2.24	Kurucz	-2.55
Cr I λ 4738.213	7.94	-3.11	NIST	...
Cr I λ 4738.460	7.94	-2.63	NIST	...

Table 8—Continued

Line	χ (eV)	$\log gf_{\gamma_{\text{Cyg}}^{\text{a}}}$	$\log gf_{\text{Sun}}^{\text{b}}$	$\log gf_{\text{Arcturus}}^{\text{c}}$	$\log gf_{\text{Source}}$	Source	$\log gf_{\text{adopted}}$
Mn I λ 4739.110	2.94	-0.48	-0.62	-0.70	-0.49	NIST	-0.48
Zr I λ 4739.480	0.65	-0.13	-0.13	-0.13	0.23	Kurucz	-0.13
Mg II λ 4739.588	11.56	-0.20	-0.66	NIST	-0.20
Ni I λ 4740.165	3.48	-1.33	-1.83	-1.85	-1.90	NIST	-1.33
Fe I λ 4740.340	3.01	-1.90	-2.67	-2.75	-2.63	NIST	-1.90
Sc I λ 4741.024	1.43	0.98	0.94	0.84	2.27	NIST	0.98
Fe I λ 4741.067	3.33	-2.48	-2.45	-2.50	-2.76	Kurucz	-2.48
Fe I λ 4741.530	2.83	-2.10	-2.10	-2.50	-1.76	NIST	-2.10
Ti I λ 4742.106	2.15	-3.96	-3.96	-3.92	-0.67	Kurucz	-3.96
C I λ 4742.561	7.94	-2.99	NIST	...
Ti I λ 4742.800	2.24	-0.09	0.01	-0.09	0.21	NIST	-0.09
Fe I λ 4742.932	4.19	-2.16	-2.36	-2.23	-2.36	Kurucz	-2.16
Fe I λ 4744.387	4.50	-0.90	-1.00	-1.10	-1.18	ccp7	-0.90
Fe I λ 4744.942	3.26	-2.45	-2.42	-2.40	-2.38	Kurucz	-2.45
Fe I λ 4745.128	2.22	-4.10	-4.05	-4.10	-4.08	NIST	-4.10
Fe I λ 4745.799	3.65	-1.25	-1.30	-1.40	-1.27	NIST	-1.25
Fe I λ 4749.947	4.55	-1.33	-1.33	-1.33	-1.33	NIST	-1.33
Fe I λ 4765.480	1.60	-3.81	-3.81	-3.70	-4.01	Kurucz	-3.81
Fe I λ 4786.806	3.01	-1.60	-1.60	-1.65	-1.60	NIST	-1.60
Fe I λ 4787.826	2.99	-2.56	-2.56	-2.50	-2.60	NIST	-2.56
Fe I λ 4788.756	3.23	-1.76	-1.76	-1.76	-1.76	NIST	-1.76

Table 8—Continued

Line	χ (eV)	$\log gf_{\gamma \text{Cyg}}^{\text{a}}$	$\log gf_{\text{Sun}}^{\text{b}}$	$\log gf_{\text{Arcturus}}^{\text{c}}$	$\log gf_{\text{Source}}$	Source	$\log gf_{\text{adopted}}$
Fe I λ 4789.650	3.54	-1.16	-1.16	-1.20	-0.96	NIST	-1.16
Fe I λ 4799.405	3.63	-1.89	-1.89	-1.93	-2.19	NIST	-1.89
Fe I λ 4802.879	3.64	-1.51	-1.51	-1.51	-1.51	NIST	-1.51
Fe I λ 4808.148	3.25	-2.84	-2.84	-2.70	-2.74	NIST	-2.84
Fe I λ 4809.938	3.57	-2.08	-2.10	-2.15	-2.60	NIST	-2.08

^aMARCS Model atmosphere with atmospheric parameters and abundances from Luck & Lambert (1981).

^bMARCS Model atmosphere with atmospheric parameters and abundances from Asplund et al. (2009).

^cMARCS Model atmosphere with atmospheric parameters and abundances from Peterson et al. (1993).

Table 9. The Fe abundances for RCB and HdC stars.

Star	$\log\epsilon(\text{Fe})^{\text{a}}$	$\log\epsilon(\text{Fe})^{\text{b}}$	$\log\epsilon(\text{Fe})^{\text{c}}$
V3795 Sgr	5.7(0.3)(3)	5.6	<6.0
XX Cam	6.8(0.3)(5)	6.8	6.8
VZ Sgr	6.1(0.3)(4)	5.8	7.2
UX Ant	6.2(0.15)(5)	6.2	7.0
RS Tel	6.5(0.2)(3)	6.4	6.9
R CrB	6.6(0.2)(5)	6.5	7.0
V2552 Oph	6.6(0.2)(4)	6.4	6.9
V854 Cen	5.0(0.3)(3)	5.0	6.5
V482 Cyg	6.7(0.15)(5)	6.7	6.9
SU Tau	6.1(0.3)(4)	6.1	6.5
V CrA	5.5(0.1)(3)	5.5	6.6
GU Sgr	6.5(0.25)(6)	6.3	6.8
FH Sct	6.4(0.15)(5)	6.3	6.8
U Aqr	6.5(0.30)(8)	...	7.3
HD 173409	6.6(0.3)(10)	6.8	6.6
HD 182040	6.6(0.25)(9)	6.9	6.4
HD 175893	6.7(0.2)(5)	6.8	6.7
HD 137613	6.8(0.20)(9)	6.6	6.7

^afrom 4700 Å region, the values in parentheses are the standard deviation and the number of lines used, respectively.

^bfrom Asplund et al. (2000) for RCB stars and from Warner (1967) for HdC stars.

^cfrom 4744.4 Å line, assuming it to be entirely Fe I.

Table 10. The derived carbon abundances for RCB stars from (0,0), (0,1) and (1,0) C₂ bands.

rs	log ϵ (C) from (0,1) C ₂ band			log ϵ (C) from (0,0)			log ϵ (C) from (1,0)			log ϵ (C) from C I lines
	C/He = 0.3%	C/He = 1.0%	C/He = 3.0%	C/He = 0.3%	C/He = 1.0%	C/He = 3.0%	C/He = 0.3%	C/He = 1.0%	C/He = 3.0%	C/He = 1.0%
	log ϵ (C) = 9.0	log ϵ (C) = 9.5	log ϵ (C) = 10.0	log ϵ (C) = 9.0	log ϵ (C) = 9.5	log ϵ (C) = 10.0	log ϵ (C) = 9.0	log ϵ (C) = 9.5	log ϵ (C) = 10.0	log ϵ (C) = 9.5
Sgr	9.0	8.9	8.8	9.0	8.8	8.7	9.0	8.8	8.6	8.9
Ant	8.4	8.3	8.2	8.2	8.1	8.0	8.4	8.1	8.0	8.7
Tel	8.4	8.3	8.3	8.7	8.5	8.4	8.7
rB	9.0	8.8	8.8	8.9	8.6	8.6	9.0	8.8	8.7	8.9
Oph	8.3	8.1	8.2	8.1	8.1	8.1	8.1	8.0	7.9	8.7
Cen	8.4	8.3	8.3	8.4	8.3	8.2	...	8.5	8.2	8.8
Cyg	8.4	8.3	8.3	8.2	8.1	8.1	8.2	8.2	8.1	8.9
Fau	8.1	8.0	8.0	7.8	7.8	7.8	7.8	7.7	7.7	8.6
rA	8.5	8.4	8.3	8.3	8.2	8.2	8.5	8.4	8.3	8.6
Sgr	8.2	8.1	8.1	8.1	8.1	8.1	8.2	8.1	8.0	8.9
Sct	7.8	7.7	7.7	7.8	7.8	7.7	7.7	7.7	7.6	8.9

Table 11. The derived carbon abundances for HdC stars and RCB star U Aqr from (0, 1) and (1, 0) C₂ bands.

stars	log ϵ (C) from (0, 1) C ₂ band			log ϵ (C) from (1, 0)			log ϵ (C) from C I lines
	C/He = 0.1%	C/He = 1.0%	C/He = 10%	C/He = 0.1%	C/He = 1.0%	C/He = 10%	C/He = 1.0%
	log ϵ (C) = 8.5	log ϵ (C) = 9.5	log ϵ (C) = 10.5	log ϵ (C) = 8.5	log ϵ (C) = 9.5	log ϵ (C) = 10.5	log ϵ (C) = 9.5
D 173409	...	8.7	8.7	...	8.6
D 182040	8.8	9.0	8.9	8.8	9.0	8.9	9.0
D 175893	8.9	9.0	8.9	8.8	8.9	8.8	8.5
D 137613	8.8	9.0	8.9	8.8	9.0	8.9	8.5
U Aqr*	...	9.2	9.2	...	8.9

Adopted (T_{eff} , log g) = (5400, 0.5). If (T_{eff} , log g) = (6000, 0.5) is adopted, the derived carbon abundance is about 10.4.

Table 12. The adopted stellar parameters and the $^{12}\text{C}/^{13}\text{C}$ ratios for the analysed stars.

Star	$(T_{\text{eff}}[\text{K}], \log g[\text{cgs}], \xi_t[\text{km s}^{-1}])$	$^{12}\text{C}/^{13}\text{C}$ Ratio ^a	$^{12}\text{C}/^{13}\text{C}$ Ratio
VZ Sgr	(7000, 0.5, 7.0)	3 - 6	...
UX Ant	(6750, 0.5, 5.0)	14 - 20	...
RS Tel	(6750, 1.0, 8.0)	>60	...
R CrB	(6750, 0.5, 7.0)	>40	>40 ^b
V2552 Oph	(6750, 0.5, 7.0)	>8	...
V854 Cen	(6750, 0.0, 6.0)	16 - 24	...
V482 Cyg	(6500, 0.5, 4.0)	>100	...
SU Tau	(6500, 0.5, 7.0)	>24	...
V CrA	(6500, 0.5, 7.0)	8 - 10	4 - 10 ^c
GU Sgr	(6250, 0.5, 7.0)	>40	...
FH Sct	(6250, 0.0, 6.0)	>14	...
U Aqr	(5400, 0.5, 5.0)	110 - 120	...
HD 173409	(6100, 0.5, 6.0)	>60	...
HD 182040	(5400, 0.5, 6.5)	>400	>100 ^{d,e}
HD 175893	(5400, 0.5, 6.0)	>100	...
HD 137613	(5400, 0.5, 6.5)	>100	>500 ^e

Note. — ^a Present work, ^b Cottrell & Lambert (1982), ^c Rao & Lambert (2008),
^d Climenhaga (1960), ^e Fujita & Tsuji (1997).

Table 13. The $\log \epsilon(\text{C})$ from (0,0) and (0,1) C_2 bands, except for RS Tel which is only from (0,0) C_2 band, with C/He ratio 1%.

Star	$(T_{\text{eff}}, \log g)$	$(T_{\text{eff}}-250, \log g)$	$(T_{\text{eff}}, \log g)$	$(T_{\text{eff}}+250, \log g)$	$(T_{\text{eff}}, \log g-0.5)$	$(T_{\text{eff}}, \log g)$	$(T_{\text{eff}}, \log g+0.5)$	$\log \epsilon (\text{C I})$
VZ Sgr	(7000, 0.5)	8.3	8.8	8.8	8.4	8.9
TX Ant	(6750, 0.5)	7.9	8.3	8.3	8.0	8.7
RS Tel	(6750, 1.0)	8.1	8.3	...	8.6	8.3	8.2	8.7
R CrB	(6750, 0.5)	8.3	8.8	8.8	8.4	8.9
552 Oph	(6750, 0.5)	7.9	8.1	...	8.5	8.1	8.0	8.7
354 Cen	(6750, 0.0)	7.8	8.3	8.3	7.9	8.8
482 Cyg	(6500, 0.5)	8.1	8.3	8.7	8.6	8.3	8.2	8.9
U Tau	(6500, 0.5)	7.8	8.0	8.4	8.3	8.0	7.9	8.6
V CrA	(6500, 0.5)	8.2	8.4	8.8	8.7	8.4	8.3	8.6
GU Sgr	(6250, 0.5)	7.9	8.1	8.4	8.3	8.1	8.1	8.9
FH Sct	(6250, 0.0)	7.5	7.7	8.0	7.9	7.7	7.6	8.9

Table 13—Continued

Star	$(T_{\text{eff}}, \log g)$	$(T_{\text{eff}}-250, \log g)$	$(T_{\text{eff}}, \log g)$	$(T_{\text{eff}}+250, \log g)$	$(T_{\text{eff}}, \log g-0.5)$	$(T_{\text{eff}}, \log g)$	$(T_{\text{eff}}, \log g+0.5)$	$\log \epsilon$ (CI)
U Aqr	(5400, 0.5)	8.9	9.2	9.5	...	9.2	...	8.9
D 173409	(6100, 0.5)	8.4	8.7	9.0	...	8.7	...	8.6
D 182040	(5400, 0.5)	8.7	9.0	9.3	...	9.0	...	9.0
D 175893	(5400, 0.5)	8.7	9.0	9.3	...	9.0	...	8.5
D 137613	(5400, 0.5)	8.7	9.0	9.3	...	9.0	...	8.5